Discrete and Continuous Dynamical Systems
Vol. 43, No. 3&4, March & April 2023, pp. 1143–1174
doi:10.3934/dcds.2022182

CAUCHY-DIRICHLET PROBLEMS FOR THE POROUS MEDIUM EQUATION

Mark Bowen[1], John R. King[2] and Thomas P. Witelski[3]

[1]Faculty of Science and Engineering, Waseda University,
3-4-1 Okubo, Shinjuku-ku, Tokyo 169-8555, Japan

[2]School of Mathematical Sciences, University of Nottingham,
University Park, Nottingham, NG7 2RD, UK

[3]Department of Mathematics, Duke University,
Durham, North Carolina, 27708-0320, USA

Dedicated to Professor Juan Luis Vázquez on the occasion of his 75^{th} birthday

Abstract. We consider the porous medium equation subject to zero-Dirichlet conditions on a variety of two-dimensional domains, namely strips, slender domains and sectors, allowing us to capture a number of different classes of behaviours. Our focus is on intermediate-asymptotic descriptions, derived by formal arguments and validated against numerical computations. While our emphasis is on non-negative solutions to the slow-diffusion case, we also derive a number of results for sign-change solutions and for fast diffusion. Self-similar solutions of various kinds play a central role, alongside the identification of suitable conserved quantities. The characterisation of domains exhibiting infinite-time hole closure is a particular upshot and we highlight a number of open problems.

1. Introduction.

The porous medium equation,

$$\frac{\partial u}{\partial t} = \nabla \cdot (u^m \nabla u)\,, \tag{1}$$

has been studied very extensively in terms of both theory and applications [29, 30]. In terms of applications, non-negative solutions of (1) can, for example, represent the moisture content of groundwater diffusing through homogeneous soils [7]. For $m = 0$, (1) reduces to the classical (linear) heat equation. While we shall occasionally comment on the fast-diffusion regime $m < 0$, our primary focus here will be on the slow-diffusion regime, $m > 0$, for which (1) admits solutions with interfaces (moving boundaries) that advance with finite speed of propagation.

We shall investigate for the most part solutions to (1) in two dimensions starting from compactly supported non-negative initial data

$$u(x, y, 0) = u_0(x, y), \tag{2}$$

2020 *Mathematics Subject Classification.* Primary: 35K55, 35K20; Secondary: 35B40, 35R35.
Key words and phrases. Porous medium equation, similarity solutions, conserved quantities, nonlinear diffusion, Dirichlet problem.

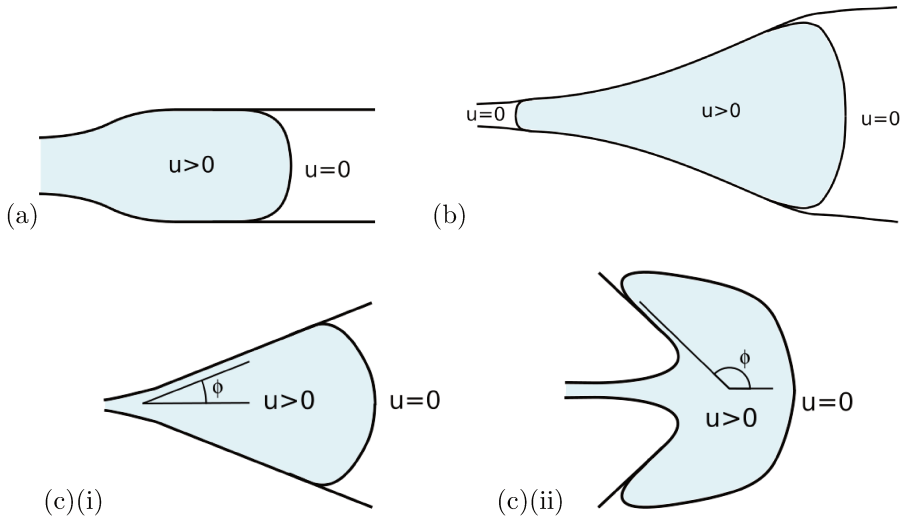

FIGURE 1. Schematics of interfaces propagating to infinity. (a) Strip-like domain. (b) Slender domains, both expanding (to the right) and contracting (to the left). (c) Wedge-like: (i) acute angle; (ii) obtuse angle; only the details of the large-time behaviour differ between acute and obtuse angles – see Section 5. In (a) and (c) the shape of the domain towards the left has negligible bearing on the large-time behaviour of the spreading to the right; the converse applies to the spreading to the left in Figure 2.

on a domain D, with $u_0 \equiv 0$ outside the initial support $\Omega_0 \subseteq D$ of u, and shall impose homogeneous Dirichlet boundary conditions on a fixed boundary ∂D

$$u = 0 \quad \text{on } \partial D. \tag{3}$$

In most cases of interest here, D will be unbounded, with the behaviour of u at infinity being context dependent; we shall adopt the convention that ∂D excludes components of the boundary at infinity. It follows from (1) and (3) that the one-dimensional quasi-steady balance

$$u^{m+1} \sim (m+1)J(s,t)(-\nu) \quad \text{as} \quad \nu \to 0^- \tag{4}$$

describes the behaviour close to ∂D at points at which the fixed boundary is smooth, where ν and s are respectively the outward normal and tangential coordinates on ∂D and J denotes the outward flux through ∂D; points at which the boundary is not smooth will be a specific focus in what follows. Incidentally, (4) highlights that $m > -1$ is required for consistency with (3).

In later sections, we will find it useful to employ two reformulations of (1). First, for $m > 0$, (1) may be rewritten in terms of the alternative dependent (pressure) variable $v = u^m$, yielding the quadratically nonlinear form [10, 16, 19]

$$\frac{\partial v}{\partial t} = v\nabla^2 v + \frac{1}{m}|\nabla v|^2, \tag{5}$$

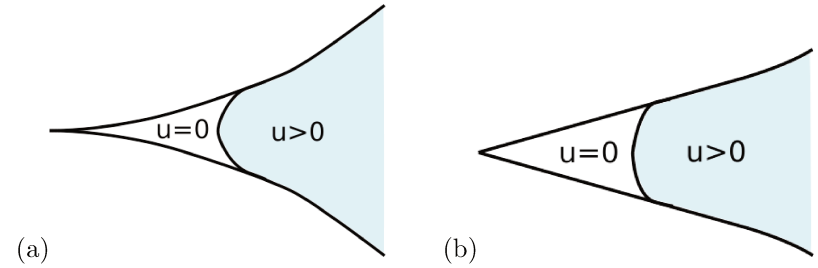

FIGURE 2. Schematics of interfaces propagating into a singular point on the boundary. (a) Cusp (locally slender domain). (b) Corner.

leading to a solution v that approaches a mass-preserving zero level set (i.e. a moving boundary) in a smooth fashion, with

$$v \sim mV_n(-\nu)_+ \quad \text{as} \quad \nu \to 0^- \tag{6}$$

where $V_n > 0$ is the speed of the moving boundary in the outward normal direction. Secondly, we note that (1) can also be written in the form

$$\frac{\partial u}{\partial t} = \frac{1}{m+1}\nabla^2\left(u^{m+1}\right), \tag{7}$$

and introducing $w = u^{m+1}$ implies

$$\frac{\partial w}{\partial t} = w^{m/(m+1)}\nabla^2 w. \tag{8}$$

In Section 5.2, we shall also consider sign-change solutions, for which (1) needs to be generalised to

$$\frac{\partial u}{\partial t} = \nabla\cdot(|u|^m\nabla u). \tag{9}$$

We now outline the contents of the remainder of the paper. Conserved quantities and self-similar solutions play a central role throughout and the relevant results are summarised in Section 2, where their role is illustrated (in tandem in the case of first-kind similarity solutions) through some known (one-dimensional and radially symmetric) examples, including of sign-change solutions. Subsequent sections explore a sequence of two-dimensional domains, illustrated schematically in Figures 1 and 2, with u subject to the zero-Dirichlet condition (3) on the fixed boundaries. For brevity, we shall largely focus on the cleanest examples in each case, but the intermediate-asymptotic (usually large-time) results are of broader applicability to domains with appropriate behaviour at infinity or at a singular point on the fixed boundary (cf. Figures 1 and 2).

Figures 3 and 4 provide numerical illustrations of the types of large-time spreading behaviours on different domains that we shall seek to quantify. These plots show results starting from typical non-negative finite mass initial conditions within the respective domains shown. Use of direct numerical simulations allows us to explore some results further. We use finite-difference schemes with adaptive time stepping to evolve the porous medium equation (1) for long times to obtain solutions that are expected to converge to self-similar forms. A robust but straightforward approach is adopted, using a nonlinear implicit finite difference method on a fixed spatially uniform rectilinear grid. We apply an Alternating Direction Implicit (ADI)-type scheme adapted to solving nonlinear parabolic equations using Newton iterations

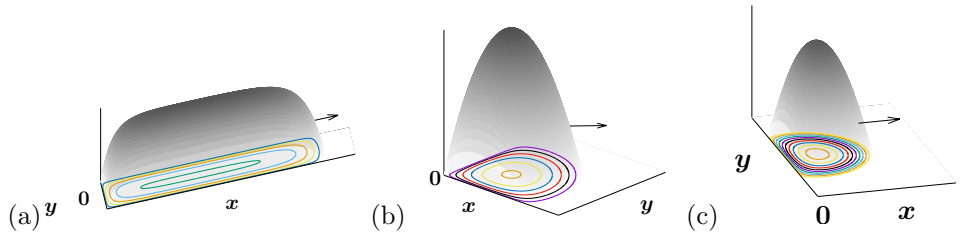

FIGURE 3. Three classes of similarity solutions for the porous medium equation on different domains: (a) on a semi-infinite strip $D = \{x \geq 0, -1 \leq y \leq 1\}$, (b) on the first quadrant $D = \{x \geq 0, y \geq 0\}$, and (c) on the half-plane $D = \{x \geq 0\}$. The profiles were computed for (1) with $m = 1$. Arrows indicate the direction of spreading further into the domain.

at each timestep [33], with adaptive time-stepping controlling the local truncation error at each time-step.

Section 3 considers two-dimensional strips (including details of the semi-infinite case) as a precursor to the investigation in Section 4 of general slender domains, and extending results of [31]. Related aspects of the generalisation to three-dimensional cylinders are outlined in the Appendix A (see also [11]); this appendix leads to a number of insights that are instructive for the analysis in the remainder of the paper. Angular sectors of small angle are natural special cases of slender domains and in Section 5 we address sectorial domains of arbitrary angle, including the special case with a smooth boundary, namely the half-plane: such domains exhibit particularly noteworthy types of behaviour. Section 5 includes a discussion of certain aspects of sign-change solutions, of interest both in their own right and as a convenient means to access additional sector angles numerically (in particular, a solution with $K-1$ lines of sign-change on a wedge of angle ϕ can be composed from K signed copies of a non-negative solution in a wedge of angle ϕ/K). Our results thus capture a wide variety of domains, including two significant transitions: firstly, and as suggested by Figure 1(b) (left-hand side) and Figure 2(a), the analysis of slender domains provides a unified description of the behaviour as the sides of the domain close off; secondly, there is a switch from finite-time to infinite-time hole closure (the scenario indicated in Figure 2(b)) as the angle of a corner on the fixed boundary decreases – that this transition is associated specifically with corner angle emphasises the broader significance of sectorial domains. Our results are all formal or numerical in nature and we conclude in Section 6 in large part by summarising issues that we believe warrant more rigorous study.

2. **Conservation laws and self-similar solutions.**

2.1. **Conserved quantities.**

We shall make substantial use of conserved quantities arising from the Laplacian operator in (7). As in [18], we consider the integral

$$M = \iint_D \Phi u \, dA, \tag{10}$$

with $\Phi = \Phi(\mathbf{x})$, so that

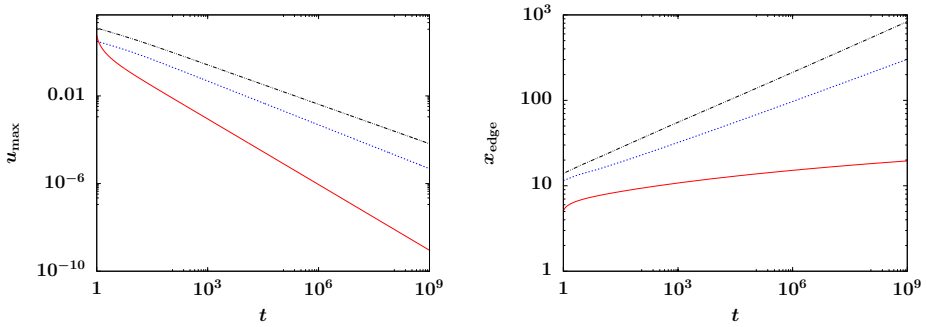

FIGURE 4. Comparing the long-time dynamics of the similarity solutions from Figure 3, on (a) the semi-infinite strip (red solid curves), (b) first quadrant (blue dashed curves), (c) half-plane (black dot-dashed curves): (left) all three approach power-law decays $O(t^{-\alpha})$ for the maximum of the solution, $u_{\max}(t) = \max_D u(x,y,t)$, but (right) while solutions (b,c) approach power-law spreading of the region of support $O(t^{\beta})$ for $x_{\text{edge}}(t) = \text{argmax}_D\{u(x,y,t) > 0\}$, the edge of support of solution (a) advances logarithmically.

$$\frac{d}{dt}\iint_D \Phi u\, dA = \frac{1}{m+1}\left(\oint_{\partial D}\left[\Phi\,\mathbf{n}\cdot\nabla(u^{m+1})\,ds - u^{m+1}\,\mathbf{n}\cdot\nabla\Phi\right]ds + \iint_D u^{m+1}\nabla^2\Phi\, dA\right), \quad (11)$$

where $\mathbf{n}$ is the unit outward normal to ∂D and any contributions to the line integral at infinity are assumed to vanish, an issue to which we need to return if the support of u is unbounded. Requiring Φ to satisfy

$$\nabla^2\Phi = 0 \text{ in } D \qquad \text{with } \Phi = 0 \text{ on } \partial D, \quad (12)$$

we obtain

$$\iint_D \Phi u\, dA = \iint_D \Phi u_0\, dA, \quad (13)$$

defining a constant of motion for the dynamics. It is important to note that in unbounded domains (12) may have non-trivial solutions; this is not usually the case, i.e. there are typically no suitable conserved quantities on bounded domains, though see the discussion of hole closure below (and (65) in particular).

As in [21], for each choice of $\Phi(\mathbf{x}) = \Phi(x,y)$, we can re-write (7) as

$$\frac{\partial}{\partial t}(\Phi u) = \frac{1}{m+1}\nabla\cdot\left[\Phi\nabla(u^{m+1}) - u^{m+1}\nabla\Phi\right]. \quad (14)$$

This conservative form could be useful for certain numerical schemes since it would, with a suitable discretisation, explicitly ensure that (10) will be conserved by the numerical solution (it is usually the case that the divergence form implemented numerically corresponds to (1), i.e. to $\Phi \equiv 1$; in this sense (14) has perhaps been under-exploited for other Φ).

2.2. **Similarity solutions.** Equation (1) admits self-similar solutions of the form

$$u(x,y,t) = t^{-\alpha}U(\xi,\eta) \qquad \xi = \frac{x}{t^{\beta}} \qquad \eta = \frac{y}{t^{\beta}}, \quad (15)$$

provided the relation

$$m\alpha + 2\beta = 1 \tag{16}$$

between the scaling exponents is satisfied. Because of the three translation invariants of (1), solution (15) can be generalised to

$$u(x,y,t) = (t-t_*)^{-\alpha} U\left(\frac{x-x_*}{(t-t_*)^\beta}, \frac{y-y_*}{(t-t_*)^\beta}\right) \tag{17}$$

for constants $t_\star$, $x_\star$ and $y_\star$, a generalisation of which we shall have cause to make use of on occasion. The similarity profile $U(\xi,\eta)$ then satisfies the quasilinear elliptic PDE

$$-\alpha U - \beta\left(\xi\frac{\partial U}{\partial \xi} + \eta\frac{\partial U}{\partial \eta}\right) = \frac{\partial}{\partial \xi}\left(U^m\frac{\partial U}{\partial \xi}\right) + \frac{\partial}{\partial \eta}\left(U^m\frac{\partial U}{\partial \eta}\right). \tag{18}$$

A second relation is required in order to determine α and β. If the relationship arises via a conservation law for the PDE, the similarity solution is said to be of the first kind [6]. If such a conserved form is not available, then α and β may need to be determined by solving (usually numerically) a nonlinear eigenvalue problem for (18); in such cases the exponents are termed anomalous and the similarity solution is referred to as being of the second kind, again see [6]. Finally, if the second relation is instead determined by the boundary conditions, then we shall follow [21] in terming the similarity solution zeroth kind.

Equation (18) inherits one of the two scaling invariants of (1), namely invariance under

$$\xi \to L\xi \qquad \eta \to L\eta \qquad U \to L^{2/m}U. \tag{19}$$

The required solution to (18) is often determined only up to this scaling, though for specific initial-boundary value problems it can (in the case of first-kind self-similarity) be specified unambiguously in terms of the initial data using the conserved quantity.

Since conservation laws and similarity reductions will play key roles in our results, we briefly recall two well-known examples for comparison. First, for the two-dimensional Cauchy problem with initial data of finite mass M_0 we take $\Phi = 1$ in (11), giving

$$\iint_{\mathbb{R}^2} u\,dxdy = \iint_{\mathbb{R}^2} u_0\,dxdy \equiv M_0;$$

for this integral of $u(x,y,t)$ to be constant requires that

$$\alpha = \frac{1}{m+1} \qquad \beta = \frac{1}{2(m+1)}, \tag{20}$$

in (15); this yields the classic Barenblatt-Pattle similarity solution [4,27,36]. This is a first-kind non-negative radially symmetric similarity solution that can be written in closed form for all $m > 0$ and any dimension $N \geq 1$. For the Cauchy problem, $\Phi = x$ and $\Phi = y$ give additional conservation laws that can be used to specify x_*, y_* in (17) via the first-moment constraints

$$\iint_{\mathbb{R}^2} (x-x_*)u_0\,dxdy = \iint_{\mathbb{R}^2} (y-y_*)u_0\,dxdy = 0.$$

Imposing these constraints enhances the large-time algebraic decay rate for the convergence of the solution of the Cauchy problem to the self-similar form [1,9,32,34].

Secondly, the Cauchy-Dirichlet problem for the porous medium equation in one dimension, on $x \geq 0$,

$$\frac{\partial u}{\partial t} = \frac{\partial}{\partial x}\left(u^m \frac{\partial u}{\partial x}\right) \qquad \text{with } u = 0 \text{ at } x = 0$$

has a first-kind similarity solution of the form

$$u(x,t) = t^{-\alpha} U(\xi) \qquad \xi = \frac{x}{t^\beta} \qquad \alpha = \frac{1}{m+1} \qquad \beta = \frac{1}{2(m+1)} \tag{21}$$

resulting from the conservation of $\Phi = x$, i.e. $M_1 = \int_0^\infty xu\,dx$. A closed-form expression for $U(\xi)$, called the dipole solution, was found in [35] as

$$U(\xi) = \left[\frac{m}{2(m+2)} \xi^{m/(m+1)} ({\xi_0}^\gamma - \xi^\gamma)_+\right]^{1/m} \tag{22}$$

with $\gamma = (m+2)/(m+1)$. For the long-time behaviour starting from initial data u_0, ξ_0 is fixed by the initial conditions through $M_1 = \int_0^\infty xu_0\,dx$ as

$$\xi_0^{2/m} = \frac{2^{1/m}(m+2)^{1/m}(2m+3)\Gamma(3+\frac{1}{m}-\frac{1}{m+2})}{m^{1/m}(m+1)\Gamma(1+\frac{1}{m})\Gamma(3-\frac{1}{m+2})}\, M_1\,.$$

As noted in [14], the dipole solution generalises to higher dimensions ($N > 1$) as

$$u = t^{-\alpha} U(\boldsymbol{\rho}), \quad \beta = \frac{1}{(N+1)(m+1)-(N-1)}\,, \qquad \alpha = (N+1)\beta\,, \tag{23}$$

where $\boldsymbol{\rho} = \mathbf{x}/t^\beta$, giving first-kind similarity solutions of the Cauchy-Dirichlet problem on the half-space $x > 0$ in N dimensions, with $\Phi = x$ again generating the relevant (first) conserved quantity.

No closed-form expression for the dipole solution is known except (22) for the $N = 1$ case. In this paper, our focus is on several classes of two-dimensional Cauchy-Dirichlet problem with no closed-form solutions and their investigation using formal asymptotics and numerical methods. The half-plane dipole solution will be revisited in the broader context of sectorial domains in Section 5.1.

3. **Two-dimensional strips.**

To describe the large-time behaviour of solutions on strips with Dirichlet boundary conditions, we begin by recalling the problem for the similarity solution of (1) on a finite domain. This will be seen to seen to be closely related to the solutions on infinite and semi-infinite strips.

3.1. **Finite-domain self-similar solutions.**

A separable solution of (1) on the interior of a finite domain D can be found in the form

$$u(x,y,t) = t^{-1/m} U(x,y) \tag{24}$$

(namely, $\alpha = 1/m$ and $\beta = 0$ in (15)), describing the large-time behaviour (see [3]). This is a zeroth-kind example, with no suitable conservation law being available and with $\beta = 0$ being required for compatibility of the similarity reduction with the boundary data. U then satisfies the boundary value problem for an autonomous nonlinear elliptic equation

$$-\frac{1}{m} U = \nabla \cdot (U^m \nabla U) \quad \text{in } D \qquad \text{with } U = 0 \text{ on } \partial D. \tag{25}$$

This problem has been studied extensively in connection with the porous medium equation, see for example [30]. The one-dimensional version of this problem plays an important role in the next two subsections.

3.2. **The advancing front solution.** Results of [31] and [11] are of direct relevance to what follows, though we shall seek to keep the analysis here self-contained. As described in [31], a steady-profile 'travelling-wave' solution on a strip can be found by assuming the form

$$u = t^{-1/m} f(z, y), \quad z = x - q \ln t \tag{26}$$

and solving the elliptic free boundary problem for

$$-\frac{1}{m} f - q \frac{\partial f}{\partial z} = \frac{\partial}{\partial z}\left(f^m \frac{\partial f}{\partial z} \right) + \frac{\partial}{\partial y}\left(f^m \frac{\partial f}{\partial y} \right) \tag{27}$$

subject to

$$f = 0 \qquad \text{at} \quad y = \pm 1, \tag{28a}$$

$$f \sim F(y) \qquad \text{as} \quad z \to -\infty, \tag{28b}$$

$$f = 0, \quad f^m \frac{\partial f}{\partial \nu} = 0 \qquad \text{at} \quad z = s(y) \tag{28c}$$

where $\partial/\partial\nu$ is the outward normal derivative at the free boundary $z = s(y)$, with $f \equiv 0$ for $z > s(y)$. Here, $F(y)$ on $-1 \le y \le 1$ is given by the solution of

$$-\frac{1}{m} F = \frac{d}{dy}\left(F^m \frac{dF}{dy} \right) \qquad \text{with } F(\pm 1) = 0, \tag{29}$$

so that F is the one-dimensional separable solution (sometimes termed the Friendly Giant – see [30], for example). The more general relevance of f lies in its role in describing an interior layer in the large-time behaviour of strip problems (Section 3.3 providing such an example). The wavespeed q in the above should be viewed as an eigenvalue, but the availability of a conserved quantity allows its explicit calculation; introducing the harmonic function

$$\Phi = e^{\pi z/2} \cos(\pi y/2)$$

solving (12) on the domain implies

$$-\frac{\partial}{\partial z}(q\Phi f) + \left(\frac{\pi}{2} q - \frac{1}{m} \right) \Phi f = \nabla \cdot \left(\Phi f^m \nabla f - \frac{1}{m+1} f^{m+1} \nabla \Phi \right),$$

and the divergence theorem then requires

$$q = \frac{2}{m\pi}, \tag{30}$$

given that Φ, $f \ge 0$. A generalisation of the first of (28) to

$$\frac{\partial f}{\partial y} = \mp \mu f \qquad \text{at} \quad y = \pm 1, \tag{31}$$

implies $\Phi = e^{\lambda z} \cos(\lambda y)$ with λ given by $\lambda \tan \lambda = \mu$ and q by $q = 1/m\lambda$, as in (96) (see Appendix A).

3.3. **The semi-infinite strip.** We now consider the initial-boundary value problem for (1) on $D = \{(x, y)|x \geq 0, -1 \leq y \leq 1\}$ with

$$\begin{aligned} u &= 0 \qquad \text{at} \quad y = \pm 1, \\ u &= 0 \qquad \text{at} \quad x = 0, \\ u &= u_0(x, y) \qquad \text{at} \quad t = 0, \end{aligned} \tag{32}$$

with $u_0 \equiv 0$ for x sufficiently large, firstly for $m > 0$ (see Figure 5 for illustrative numerical results), and then for $m = 0$ and $-1 < m < 0$. Introducing

$$\Phi = \sinh\left(\frac{\pi x}{2}\right)\cos\left(\frac{\pi y}{2}\right)$$

yields

$$\int_0^\infty \int_{-1}^1 \Phi(u - u_0)\, dydx = 0 \tag{33}$$

and the $t \to +\infty$ structure involves the following two main regions: firstly,

$$u \sim t^{-1/m} g(x, y) \quad \text{for} \quad x = O(1), \tag{34}$$

with

$$\begin{gathered} -\frac{1}{m} g = \frac{\partial}{\partial x}\left(g^m \frac{\partial g}{\partial x}\right) + \frac{\partial}{\partial y}\left(g^m \frac{\partial g}{\partial y}\right), \\ \begin{aligned} g &= 0 \qquad \text{at} \quad x = 0, \\ g &\sim F(y) \qquad \text{as} \quad x \to +\infty, \\ g &= 0 \qquad \text{at} \quad y = \pm 1, \end{aligned} \end{gathered}$$

with $F(y)$ given by (29). Secondly, (26)-(28) hold for $z = O(1)$, with z defined as in (26) and with (30) alternatively following from (33).

The compatibility of these two in the sense of matched asymptotic expansions is implicit in (28b). Since formal matching arguments will play a central role in the current analysis, we elaborate here on how such arguments proceed. The large-time asymptotic structure in the current case should in fact be viewed as comprising three regions: (i) a boundary layer region $x = O(1)$ described at leading order by (34), (ii) an interior layer $x = q \ln t + O(1)$ governed at leading order by (26) and (iii) an outer region $x = O(\ln t)$ with $0 < x/\ln t < q$ in which the leading-order behaviour is one-dimensional, given by $u \sim t^{-1/m} F(y)$. Two examples of inner/outer matching thus arise here: as $x \to \infty$ in (i) we recover the limiting behaviour of (iii) as $x/\ln t \to 0^+$, while the $z \to -\infty$ limit of (ii) coincides with the limit $x/\ln t \to q^-$ of (iii). Since the leading-order solution in (iii) is independent of x, both of these examples of matching are straightforward, but the above comments may nevertheless serve to clarify how such matching arguments proceed (see [17] for example, for detailed descriptions of the principles of matched asymptotics).

We note that the formulation of Section 3.2 determines f only up to translations of z; (33) in principle allows its complete specification.

For the (linear-diffusion) borderline case $m = 0$ the large-time behaviour is given by

$$u \sim K t^{-3/2} e^{-\pi^2 t/4} \cos\left(\frac{\pi y}{2}\right) x e^{-x^2/4t} \quad \text{as} \quad t \to +\infty \quad \text{with} \quad x = O(t^{1/2}), \tag{35}$$

where the constant K is given by

$$\pi^{3/2} K = \int_{-1}^1 \int_0^\infty \sinh\left(\frac{\pi x}{2}\right)\cos\left(\frac{\pi y}{2}\right) u_0(x, y)\, dxdy.$$

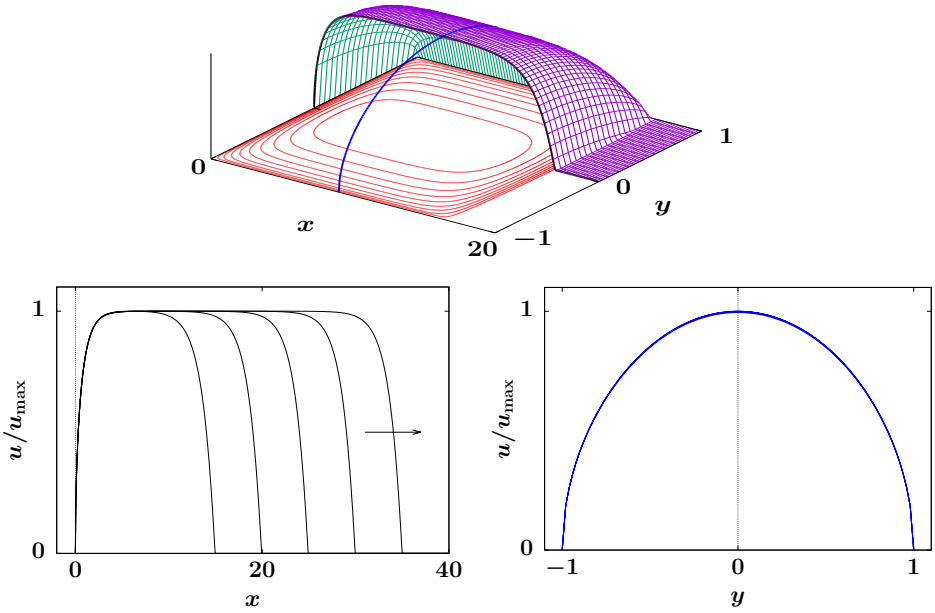

FIGURE 5. Computed solutions on the semi-infinite strip for $m = 1$. (top) 3-D cut-away view of $u(x, y, t)$ (axes not to scale), cross-sections being indicated by the blue and black curves. (left) Time profiles of the scaled centreline profile, $u(x, 0, t)/u_{\max}(t)$ at increasing times, (right) Scaled cross-section profiles mid-way through the computed PDE solution, $u(x_{\text{edge}}(t)/2, y, t)/u_{\max}(t)$, at corresponding times, consistent with the 1-D zeroth-kind separable solution $F(y)$ of (29).

For fast diffusion with $m \in (-1, 0)$, we conjecture (by analogy with results of Appendix A and on the basis of an asymptotic analysis of the limiting behaviour as $m \to 0^-$ and $m \to -1^+$) that the separable solution

$$u \sim (t_c - t)^{1/(-m)} f(x, y) \quad \text{as} \quad t \to t_c^- \tag{36}$$

describes the intermediate-asymptotic behaviour in the sense of [6] (the asymptotic behaviour for $t > t_c$ being simply $u \equiv 0$; no additional regimes are needed in this case) for a positive constant t_c that depends on the initial data and with

$$u^{1+m} \sim a(t) e^{-\pi x/2} \cos\left(\frac{\pi y}{2}\right) \quad \text{as} \quad x \to +\infty$$

for all t for compactly supported initial data, for example, from which the far-field behaviour (36) should be apparent. We shall not take the analysis of the fast-diffusion case any further here, however.

We conclude this section with an aside that we shall also not pursue further here. For Robin conditions (see (75)), a systematic formal asymptotic procedure leads to (as in Appendix A)

$$\frac{\partial u}{\partial t} = \frac{\partial}{\partial x}\left(u^m \frac{\partial u}{\partial x}\right) - \mu u^{m+1} \tag{37}$$

as $\mu \to 0$, with t scaling with $1/\mu$ and x with $1/\mu^{1/2}$. However, an ad hoc procedure based on vertical integration could also be adopted for any μ (including $\mu = \infty$) to

achieve a similar reduction in dimensionality, as follows. We have the exact result

$$\frac{\partial}{\partial t}\left(\int_{-1}^{1}\cos(\lambda y)u\,dy\right)= \frac{1}{m+1}\frac{\partial^2}{\partial x^2}\left(\int_{-1}^{1}\cos(\lambda y)u^{m+1}\,dy\right)-\frac{\lambda^2}{m+1}\int_{-1}^{1}\cos(\lambda y)u^{m+1}\,dy$$

for $\lambda\tan\lambda=\mu$. If we now approximate u within these integrals in the form

$$u\approx F(y)U(x,t), \tag{38}$$

where F is given by (29), except that the boundary conditions are replaced by

$$\frac{dF}{dy}=\mp\mu F \qquad \text{at} \quad y=\pm 1,$$

then it follows that

$$\int_{-1}^{1}\cos(\lambda y)F^{m+1}\,dy=\frac{m+1}{m\lambda^2}\int_{-1}^{1}\cos(\lambda y)F\,dy,$$

allowing closure of the formulation for U in the form

$$\frac{\partial U}{\partial t}=\frac{m+1}{m\lambda^2}\frac{\partial}{\partial x}\left(U^m\frac{\partial U}{\partial x}\right)-\frac{1}{m}U^{m+1}.$$

This is consistent with (37) in the limit $\mu\to 0$ and, moreover, has the correct x-independent separable solution for u. We note that achieving such a closure places severe constraints on both the choice of weighting function (i.e. $\cos(\pi y/2)$) in the vertical integration and on the choice of the y-dependent profile in (38).

4. **Slender domains.** In this section we generalise the results of Section 3 by considering boundaries that vary slowly in the x direction. This will provide a rather general description of slender domains, and one that encompasses small-angle wedges, representing a bridge to the results of Section 5. Here we consider only $m>0$ and set

$$u=0 \qquad \text{at} \quad y=\pm h(\varepsilon x)$$

with $0<\varepsilon\ll 1$, focussing on the symmetric case here for brevity; the approach again readily generalises (including to domains whose centreline is not straight). Setting $X=\varepsilon x$, potential conserved quantities can be constructed by the Liouville-Green method in the form

$$\Phi\sim e^{\pm\sigma(X)/\varepsilon}\cos(\sigma'(X)y) \tag{39}$$

with

$$\sigma'(X)=\frac{\pi}{2h(X)}. \tag{40}$$

Adopting a direct approach before revisiting (39), we set

$$u=t^{-1/m}\psi(X,y), \quad \tau=\varepsilon\ln t \tag{41}$$

to give

$$\varepsilon\frac{\partial\psi}{\partial\tau}-\frac{1}{m}\psi=\frac{\partial}{\partial y}\left(\psi^m\frac{\partial\psi}{\partial y}\right)+\varepsilon^2\frac{\partial}{\partial X}\left(\psi^m\frac{\partial\psi}{\partial X}\right).$$

Local to the midpoint of the moving boundary, defined to be $X=S(\tau)$, we rescale according to

$$y=h(S)Y, \quad X=S(\tau)+\varepsilon h(S)Z, \quad \psi=h^{2/m}(S)\Psi(Z,Y)$$

to give

$$\frac{\varepsilon}{h^{2/m}(S)}\frac{\partial}{\partial\tau}\left(h^{2/m}(S)\Psi\right)-\varepsilon\frac{h'(S)}{h(S)}\frac{dS}{d\tau}\left(Z\frac{\partial\Psi}{\partial Z}+Y\frac{\partial\Psi}{\partial Y}\right)-\frac{1}{m}\Psi$$
$$-\frac{1}{h(S)}\frac{dS}{d\tau}\frac{\partial\Psi}{\partial Z}=\frac{\partial}{\partial Z}\left(\Psi^m\frac{\partial\Psi}{\partial Z}\right)+\frac{\partial}{\partial Y}\left(\Psi^m\frac{\partial\Psi}{\partial Y}\right).$$

Hence

$$\Psi\sim f(Z,Y)$$

with f given as in (27)-(28), with (30) therefore requiring

$$\frac{1}{h(S)}\frac{dS}{d\tau}\sim\frac{2}{m\pi}. \tag{42}$$

Equivalently, (39), (41) imply

$$\sigma(S)\sim\frac{1}{m}\tau,$$

rendering (40) and (42) equivalent.

While the above results are general, it is instructive to conclude this section by considering two specific forms for $h(X)$, as follows.

Case (I):

$$h(X)\sim\kappa X^\gamma\quad\text{as}\quad X\to+\infty\quad\text{with}\quad\gamma\le 1. \tag{43}$$

The case $\gamma=0$ corresponds to that of Section 3.3, while $\gamma=1$ arises for a wedge of small angle; wedges capture an important transition in behaviour and are analysed in Section 5 below. Figure 1(b) provides a schematic of such cases, with $\gamma>0$ on the right and $\gamma<0$ on the left. We note that when $\gamma<0$ the expression (43), as well as (46) below with $\gamma>1$, corresponds to a slender limit whether or not the small parameter ε is introduced at the start for ease of accounting. When (43) applies we obtain

$$S(\tau)\sim\left(\frac{2(1-\gamma)\kappa}{m\pi}\tau\right)^{1/(1-\gamma)}\quad\text{as}\quad\tau\to+\infty,\quad\gamma<1, \tag{44}$$

$$S(\tau)\sim S_\infty\exp\left(\frac{2\kappa}{m\pi}\tau\right)=S_\infty t^{2\kappa\varepsilon/(m\pi)}\quad\text{as}\quad\tau\to+\infty,\quad\gamma=1, \tag{45}$$

for some constant S_∞ that will depend on the initial data. The propagation is thus logarithmic in t in the former case, but of power-law type in the latter (consistent with Section 5).

Case (II):

$$h(X)\sim\kappa(X-X_0)^\gamma\quad\text{as}\quad X\to X_0^+\quad\text{with}\quad\gamma\ge 1. \tag{46}$$

Figure 2(a) represents the schematic relevant to this case. Here

$$S(\tau)-X_0\sim\left(\frac{2(\gamma-1)\kappa}{m\pi}\tau\right)^{-1/(\gamma-1)}\quad\text{as}\quad\tau\to+\infty,\quad\gamma>1, \tag{47}$$

$$S(\tau)-X_0\sim S_\infty\exp\left(-\frac{2\kappa}{m\pi}\tau\right)\quad\text{as}\quad\tau\to+\infty,\quad\gamma=1. \tag{48}$$

A particular consequence of the above is for the well-studied finite-domain case in which the large-time behaviour is known to be separable (see Section 2); the implication of (47)-(48) is that this behaviour need not be uniformly valid for domains whose boundary contains one or more outward-facing cusp or corner of sufficiently small angle – when $u\equiv 0$ holds initially in the neighbourhood of such a singularity

the moving boundary does not fully encroach onto the fixed boundary in finite time. In Section 5, we determine the critical angle for such behaviour.

More exotic forms of $h(X)$ are readily analysed on the basis of (42), allowing arbitrarily weak dependence upon τ, for example.

5. **Sectorial domains.** We now consider the Cauchy-Dirichlet problem for (1) in sectors with opening angle 2ϕ. In general these results will be most conveniently expressed in polar coordinates on $D = \{(r,\theta)\,|\,0 \le r < \infty, -\phi \le \theta \le \phi\}$ with $u = 0$ imposed on $\theta = \pm\phi$, and we use the terms sectors and wedges interchangeably to denote the domain $-\phi < \theta < \phi$. Following some introductory comments, in this section we first discuss in some detail (see Section 5.1) the half-plane case ($\phi = \pi/2$) that has been the subject of prior attention, supplementing this with numerical solutions for other specific ϕ. Section 5.2 addresses aspects of sign-change solutions. Section 5.3 elucidates a critical angle at which an important transition occurs, Section 5.4 focussing on this transition. Section 5.5 makes some brief remarks about the linear and fast diffusion cases $m \le 0$, while Section 5.6 touches on the possibility of waiting-time behaviour at a corner (for which the same critical angle is relevant). Many of the results described here are of relevance locally or in the far field to much more general domains containing a corner in the boundary or approaching a wedge as $r \to \infty$, respectively.

For any $\phi > 0$, (11) yields a sequence of conserved quantities based on the solutions of (12) that are bounded at the origin

$$\begin{cases} \Phi_n(r,\theta) = r^{\lambda_n}\cos(\lambda_n\theta) & n \text{ odd} \\ \Phi_n(r,\theta) = r^{\lambda_n}\sin(\lambda_n\theta) & n \text{ even} \end{cases} \qquad \text{with} \quad \lambda_n = \frac{n\pi}{2\phi} \tag{49}$$

for all $n \ge 1$. Taking $n = 1$, from the conservation of $M_1 \equiv \iint_D \Phi_1 u\, r dr d\theta$, we obtain non-negative first-kind self-similar solutions of the form

$$u = t^{-\alpha} U(\rho,\theta), \quad \rho = \frac{r}{t^\beta} \tag{50a}$$

with

$$\alpha = \frac{\pi + 4\phi}{m\pi + 4(m+1)\phi}, \quad \beta = \frac{2\phi}{m\pi + 4(m+1)\phi}. \tag{50b}$$

The small angle limit of this solution can be seen to agree with solution (45) on a slender wedge by setting $\phi = \kappa\varepsilon$ yielding $r \propto t^{2\phi/(m\pi)}$, consistent with the small ϕ limit of β in (50b). In the limit $\phi \to \infty$[1] the similarity parameters in (50b) approach those associated with an axisymmetric source solution (20) (i.e. the boundaries become of limited relevance).

Certain aspects of the similarity solution are more conveniently addressed in terms of the pressure form, $V = U^m(\rho,\theta)$ (based on (5)), satisfying the elliptic equation,

$$-m\alpha V - \beta\rho\frac{\partial V}{\partial \rho} = V\left(\frac{1}{\rho}\frac{\partial}{\partial\rho}\left[\rho\frac{\partial V}{\partial\rho}\right] + \frac{1}{\rho^2}\frac{\partial^2 V}{\partial\theta^2}\right) + \frac{1}{m}\left(\left[\frac{\partial V}{\partial\rho}\right]^2 + \frac{1}{\rho^2}\left[\frac{\partial V}{\partial\theta}\right]^2\right). \tag{51}$$

The support of the non-negative solution will lie within some disk centered at the origin, $0 \le \rho \le \rho^*$. Based on our numerical results, we conjecture that the maximum distance to the edge of the support is achieved on the centreline of the (symmetric)

[1] $\phi > \pi$ could in principle be realised via a closely spaced helical sheet, and is in any case mathematically meaningful.

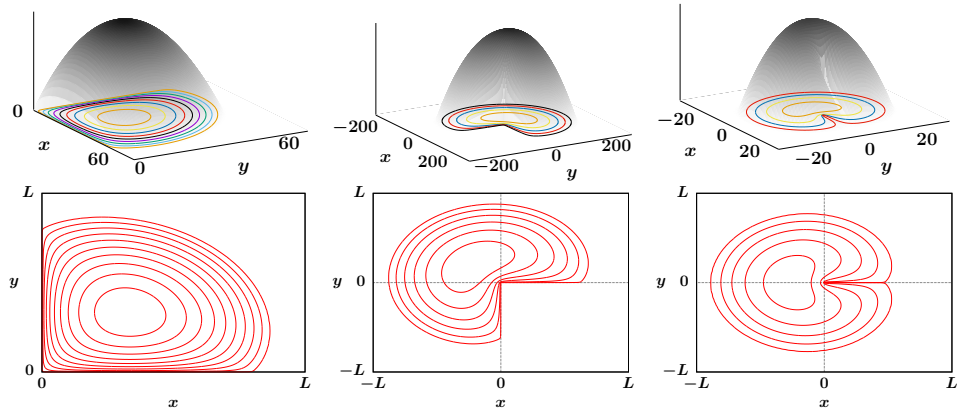

FIGURE 6. Numerically computed PDE solutions at large times for (1) with $m = 1$ for: (left) the quarter plane problem, $\phi = \pi/4$, (middle) the 3-quarter plane problem, $\phi = 3\pi/4$, and (right) the slit-plane problem, $\phi = \pi$.

solution, $\theta = 0$, that is at some ρ_0^* with the rest of the interface satisfying $0 \le \rho(\theta) \le \rho_0^*$.

Using the symmetry of the non-negative solution about the centreline, $\theta = 0$, the local expansion of $V(\rho, \theta)$ at the tip of the interface can be obtained as

$$V \sim m\beta\rho_0^*(\rho_0^* - \rho) - \frac{m}{2(1+m)}\Big(m\alpha + (1-m)\beta - 2C_0\Big)(\rho_0^* - \rho)^2 - (\rho_0^*)^2 C_0\theta^2 \quad (52)$$

for some positive tip curvature $C_0 > 0$ giving the form of interface at the tip as

$$\rho \sim \rho_0^* - \frac{\rho_0^* C_0}{m\beta}\theta^2 \qquad \text{for } \theta \to 0 \quad (53)$$

(cf. (103) and (104) for specifics of the half-plane case). Similarly, having finite-flux out through the boundaries of the sector implies local behaviours of the form

$$V \sim A(\rho)|\theta \mp \phi|^{m/(m+1)} \qquad \text{for } \theta \to \pm\phi \text{ with } \rho = O(1).$$

The forms of these local results apply for all ϕ, but notably they do not include the behaviour at the origin. The behaviour as $\rho \to 0$ is considered in Section 5.3 and is connected to the existence of a critical sector angle ϕ_c.

Our finite-difference numerical computations, described in the Introduction, directly apply to the half-plane ($\phi = \pi/2$) and quarter-plane ($\phi = \pi/4$) problems, as shown in Figure 3. The numerics are easily extended to obtain solutions on other domains expressible as rectangular polygons, such as a "re-entrant corner" (or three-quarter plane, $\phi = 3\pi/4$), and the slit-plane ($\phi = \pi$), shown in Figure 6. For numerical convenience, the domains have been rotated so that boundaries align with the coordinate axes. Apart from these special "rectangular" cases, a different approach is required in order to compute solutions on other sectors; below we make use of sign-change solutions partially to overcome this limitation.

5.1. **The half-plane solution.** For the half-plane case, $\phi = \pi/2$, (50) yields

$$\alpha = \frac{3}{3m+2} \qquad \beta = \frac{1}{3m+2}\,. \quad (54)$$

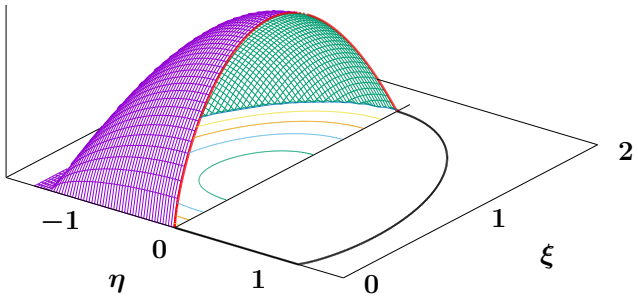

FIGURE 7. Cut-away view of the numerically computed half-plane similarity solution for $m = 2$. It is shown in terms of the pressure $V(\xi,\eta) = U(\xi,\eta)^m$. The solution is symmetric about the line $\eta = 0$. The centreline profile (red curve), $V(\xi, 0)$, and the free boundary (black curve), $V(\xi,\eta) = 0$, are shown in more detail in Figure 13.

Taking the domain D as being the right-half plane, the first few conserved integrals have $\Phi_1 = x, \Phi_2 = 2xy, \Phi_3 = (x^3 - 3xy^2)/4$.

This case is distinguished in that it is the only sector that has a translation invariance parallel to the boundary; if $u(x, y, t)$ is a solution on the right half-plane, then so is $u(x, y - y_*, t)$ for any y_*. This translation invariance does not imply that $\iint_D yu\,dA$ is conserved (it is not), but a distinguished value for y_* that enables faster convergence to the large-time behaviour can be obtained using the conserved integral for $\Phi_2 = 2xy$,

$$y_* = \frac{M_2}{2M_1} = \frac{\iint_D 2xyu\,dA}{2\iint_D xu\,dA}\,.$$

Figure 7 shows a computed representation of the non-negative similarity solution. This solution can of course be extended in an antisymmetric manner to yield a sign-change solution on the whole plane; for this reason this solution has been called the dipole solution [14]. No exact closed-form solution is available, and in Appendix B we show how local asymptotic expansions can be employed in order to gain substantial insight into several important features of the solution.

5.2. **Sign-change solutions.** Here we first briefly review to solutions to the one-dimensional version of (9) with compactly supported initial data that change sign before turning to the richer family of solutions that exist in the two-dimensional case.

In these solutions, one or more additional moving boundaries are present, associated with interior zeros of u, the local behaviour at such a location taking the form (cf. (4))

$$|u|^m u \sim -(m+1)J(t)(x - x_0(t)) \quad \text{as} \quad x \to x_0 \tag{55}$$

where $J(t)$, the flux through x_0, can take either sign. Such solutions have been investigated in some detail for the Cauchy problem (e.g. [12,13,15]); here we provide context for later comments by recording results for the half-line with $u = 0$ on $x = 0$, corresponding to odd solutions to the Cauchy problem. If the first moment of the initial data is non-zero we recover the (first-kind) dipole solution (22) described above, but if it is zero then second-kind solutions must instead be constructed: to obtain $U(\xi)$ and α it is then necessary to solve the nonlinear eigenvalue problem

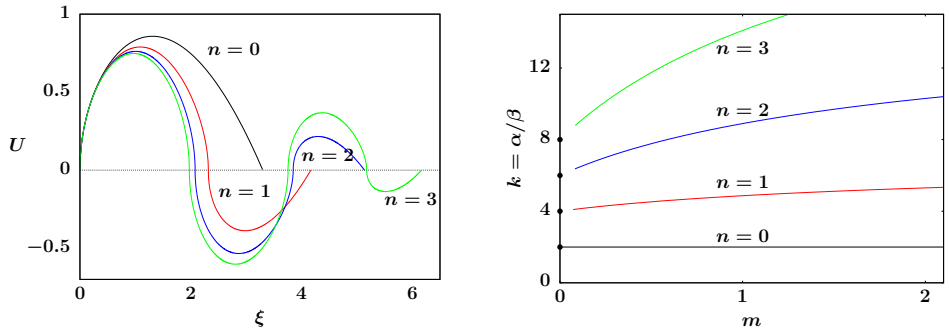

FIGURE 8. (left) Profiles with $m = 1$ for similarity solutions (the non-negative solution (black), and solutions with $n = 1, 2, 3$ sign changes (red, blue, and green curves respectively)). Solutions are normalised to satisfy condition (58). (right) The corresponding $k = \alpha/\beta$ ratios over a range of m, ending with the first-kind solution values $k_n = 2(n + 1)$ at $m = 0$.

$$-\alpha U - \frac{1}{2}(1 - m\alpha)\xi\frac{dU}{d\xi} = \frac{d}{d\xi}\left(|U|^m\frac{dU}{d\xi}\right) \qquad \text{on } 0 \le \xi \le \xi_0, \tag{56a}$$

$$U = 0 \qquad \text{at} \quad \xi = 0, \tag{56b}$$

$$U = 0 \quad |U|^m\frac{dU}{d\xi} = 0 \qquad \text{at} \quad \xi = \xi_0 \tag{56c}$$

from which it follows for $\alpha \neq 1/(m + 1)$ that

$$\int_0^{\xi_0} \xi U \, d\xi = 0. \tag{57}$$

In fact, our numerical approach imposes (57) in place of the second of (56c), the two being equivalent. In the absence of a conserved quantity, we eliminate the scaling invariance of (56a) by prescribing the coefficient of the local behaviour as $\xi \to 0$ to be one, enforcing the condition

$$U \sim \xi^{1/(m+1)} \qquad \text{as} \quad \xi \to 0. \tag{58}$$

It has been established [12, 13] that the sequence of α_n for solutions with $n = 1, 2, 3, \cdots$ sign changes is ordered,

$$\alpha_0 < \alpha_1 < \alpha_2 < \alpha_3 < \cdots, \tag{59}$$

where $\alpha_0 = 1/(m + 1)$ from (21). Figure 8 shows numerical results for $n = 0, 1, 2$ and 3. The left plot shows the profiles for $U_n(\xi)$ for $m = 1$; note that the local structure at a sign change follows (55) and is distinct from the behaviour at the edge of support, namely

$$|u|^m \sim m\frac{ds}{dt}(s - x) \quad \text{as} \quad x \to s^-(t);$$

cf. (6). The right plot shows the ratio $k = \alpha/\beta$, the rate of decay of the amplitude relative to the rate of spreading of the support, over a range of m. This ratio is constant ($k = 2$) for the first-kind solution and varies smoothly with m for each n. These curves approach the limiting values $k_n(0) = 2n + 2$ that can be obtained

analytically from taking n^{th} time derivative of the dipole similarity solution of the $m = 0$ linear problem, namely $u(x,t) = xt^{-3/2}\exp(-x^2/(4t))$.

As already noted, a single-signed solution on a sector of angle $2\hat{\phi}$ can be extended anti-symmetrically across sector edges to yield a solution with j sign-changes (occurring on equally spaced rays) in a sector of opening angle $2\phi = 2(j+1)\hat{\phi}$ for $j = 1, 2, \cdots$. The scaling exponents of the sign-changing $U(\xi,\eta)$ on half-angle $\phi = (j+1)\hat{\phi}$ are, of course, given by the α, β of the fundamental solution on $\hat{\phi}$. Applying this reasoning in reverse, we can construct non-negative solutions on a sector of angle $2\hat{\phi}$ by obtaining suitable sign-changing solutions on angle 2ϕ.

Sign-change solutions also exist with less trivial nodal curves. These will not have the same discrete-angular symmetries as the first-kind solutions described above, being of second kind: rather than the similarity exponents α and β being selected by one of the Φ_n, these will have

$$M_n = \iint_D \Phi_n u \, dA = 0$$

for any n sufficiently small that the associated first-kind solution decays more slowly than the second-kind solution in question. While almost any finite-mass, non-negative compactly supported initial data could be used in numerical simulations to converge at long times to non-negative similarity solutions, more care is needed to obtain sign-change solutions. As described in [15], generic signed initial data will evolve to extinguish sign changes and will approach single-signed solutions for long times. However, if the initial data are constructed with selected $M_n = 0$, then such properties will be preserved for all t. If the initial data are anti-symmetric across j rays at equally spaced angles, then sign-changing first-kind solutions can be obtained. If other nodal curves are imposed to make other $M_n = 0$ initially, then that sign-change structure is found to be preserved in the second-kind similarity solutions. We will illustrate these points with a few numerical simulations.

Figure 9 shows contours of numerically computed solutions of (1) with $m = 1$ in the upper half plane obtained at large times from different choices of initial data $u_0(x,y)$. For this problem, the integral $M_1 = \iint_D y u_0 \, dA$ is a conserved quantity. For the non-negative initial data in panel (a), $M_1 > 0$ and for long times the first-kind non-negative solution is approached. In panels (b) and (d) signed initial data were selected with symmetries that make $M_1 = 0$. For (b), $M_2 > 0$ and the solution decomposes into a pair of oppositely signed quarter-plane first-kind similarity solutions, corresponding to $\phi = \pi/4$. For (d), $M_2 = 0$ but $M_3 > 0$ and the solution decomposes into a set of three identical (except for alternating signs) first-kind solutions for $\phi = \pi/6$. In contrast, the initial data for panel (c) in Figure 9 were selected to be symmetric across the x-axis and to change sign across a line $y = y_c > 0$ so that the integrals on $0 \le y \le y_c$ and $y_c \le y < \infty$ comprising M_1 cancel, yielding $M_1 = 0$. Consequently, this evolves to a second-kind similarity solution. While plots of $u_{\max}(t)$ (as in Figure 4a) for the other solutions in the figure accurately match the decay rates predicted by the similarity solutions,

$$\alpha_a = \frac{3}{5}, \qquad \alpha_b = \frac{4}{6}, \qquad \alpha_d = \frac{5}{7},$$

for (c) the decay rate was estimated by fitting to simulation data on the range $100 \le t < 10^8$ to yield $\alpha_c \approx 0.7108$. This is close to, but distinct from, the other α values. Sign-change solutions are expected to be unstable over very long times

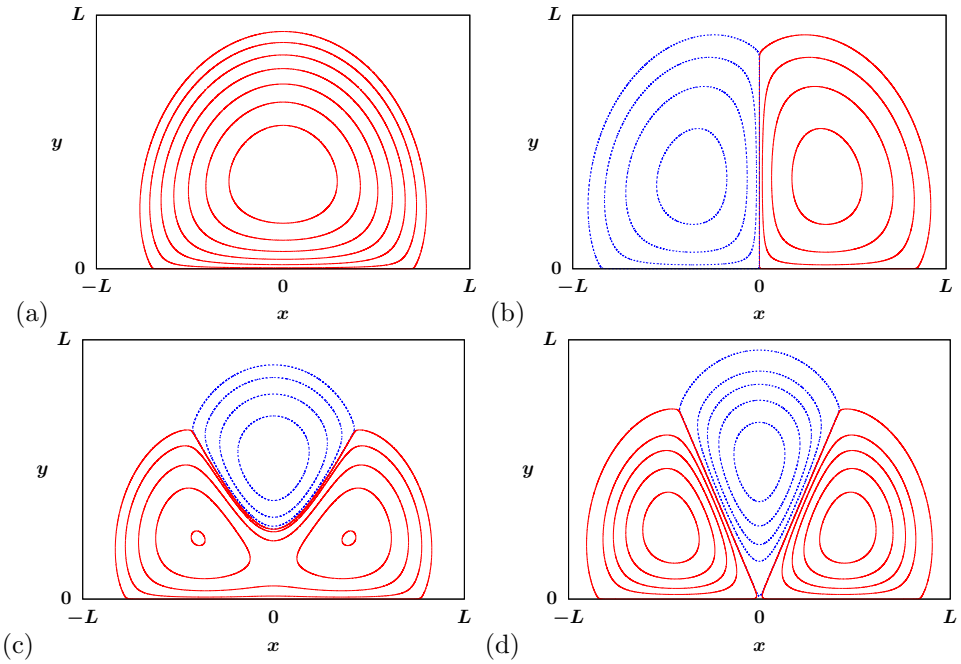

FIGURE 9. Numerical simulations of (9) with $m = 1$ in the upper half plane, showing contours of the self-similar solution at a typical large time, starting from different initial data: (a) the non-negative half-plane solution, (b) a pair of oppositely signed quarter plane solutions (contours corresponding to positive solution values are shown as solid red curves, while contours for negative solution values are shown as blue dashed curves), (c) a second-kind similarity solution with a single non-trivial nodal curve, (d) three sectorial solutions with angle $\phi = \pi/6$ with alternating signs.

to numerical instabilities that break their symmetries, likely driving it to evolve towards a different similarity solution.

Similarly, Figure 10 shows contours of numerically computed solutions for (1) with $m = 1$ in the quarter plane, $\phi = \pi/4$, obtained at large times from different choices of initial data $u_0(x, y)$. For this problem on the first quadrant, the integral $M_1 = \iint_D (x^2 - y^2) u_0 \, dA$ is a conserved quantity (recall, though, that the coordinate system in Figure 10 is rotated from that elsewhere – for the coordinate system shown in the figure $\Phi_1 = 2xy$ applies). The non-negative first-kind solution, with $M_1 > 0$, is presented in Figure 9b. All of the plots in Figure 10 have $M_1 = 0$, but they differ after that. In panel (a), $M_1 = 0$ by virtue of being anti-symmetric across the line $y = x$, yield the solution as a pair of identical oppositely signed first-kind similarity solutions for $\phi = \pi/8$, with $M_2 > 0$ with $\phi = \pi/4$ in (49). In panel (b), $M_1 = 0$ based on oppositely signed portions of the initial data close to and further from the origin and symmetric about the midline: this is a second-kind solution on $\phi = \pi/4$. Panel (c) shows another second-kind solution, having sign changes across the line $y = x$ and on a curve passing orthogonally through that line. This yields a solution that decomposes into two identical oppositely signed second-kind

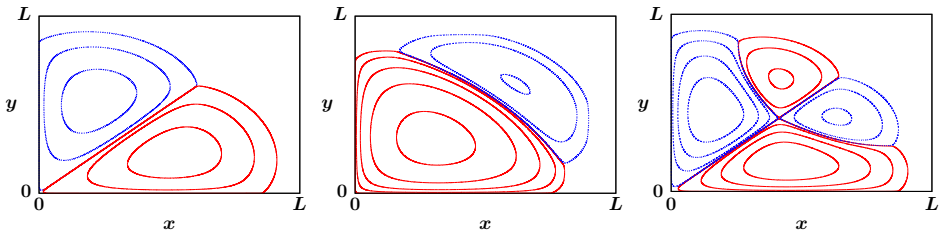

FIGURE 10. Numerical simulations of (9) with $m = 1$ in the quarter plane given by the first quadrant, showing contours of the self-similar solution at a typical large time, starting from different initial data: (left) a pair of oppositely signed $\phi = \pi/8$ sector first-kind similarity solutions, (middle) a second-kind similarity solution with a single non-trivial nodal curve, (right) a pair of oppositely signed $\phi = \pi/8$ second-kind similarity solutions.

solutions on $\phi = \pi/4$. As in Figure 9, we expect such solutions to be unstable to perturbations that break its symmetries.

These solutions were observed to be maintained for long-times in numerical simulations, and yielded scalings for $u_{\max}(t)$ with

$$\alpha_a = \frac{6}{8}, \qquad \alpha_b \approx 0.7922, \qquad \alpha_c \approx 0.8392$$

fitted on $10^4 \leq t < 10^{12}$. Figures 9 and 10 illustrate how simulations of sign-change solutions on rectangular domains can be used to obtain non-negative solutions on smaller sectors.

5.3. **The critical angle ϕ_c.** We now show that the local structure at the vertex of the sector defines a critical angle $\phi_c(m)$, namely

$$\phi_c(m) = \frac{m\pi}{4(m+1)}, \tag{60}$$

or equivalently a critical exponent m in (1) for solutions on a sector of angle ϕ,

$$m_c(\phi) = \frac{4\phi}{\pi - 4\phi} \quad \text{for} \quad \phi < \pi/4. \tag{61}$$

We will show that ϕ_c provides, for example, a bound on vertex-opening-angle ϕ for which a hole (i.e. a region in which $u \equiv 0$) local to the vertex can close in finite time. The limits of ϕ_c are instructive, with $\phi_c \to 0^+$ as $m \to 0^+$ and $\phi_c \to \pi/4^-$ as $m \to +\infty$ (also see Figure 11), the latter corresponding to the Hele-Shaw problem, which is of independent interest.

We now distinguish the behaviour according to whether ϕ is greater than or less than ϕ_c. In the course of what follows we shall establish a number of distinct arguments leading to the identification of (60).

(A) Large angles: $\phi > \pi m/4(m+1)$.

The first way in which we identify ϕ_c as the critical angle arises as follows: for $\phi > \phi_c$, once $u > 0$ holds in the neighbourhood of the corner (this necessarily occurs in finite time for $\phi > \phi_c$) the quasi-steady local balance

$$u \sim \left(A(t) r^{\pi/2\phi} \cos(\pi\theta/2\phi) \right)^{1/(m+1)} \quad \text{as} \quad r \to 0 \tag{62}$$

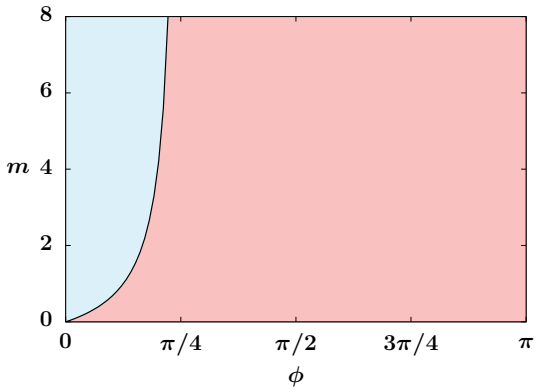

FIGURE 11. Diagram of (m, ϕ)-space illustrating the different regions corresponding to the two possible leading order terms at the vertex of sectors. The separating curve is given by critical sector angle (60)

pertains, the condition on ϕ being a prerequisite for the self-consistency of such a balance, since the right-hand side of (1) scales with $r^{(\pi-4\phi)/2\phi}$ and the left-hand side with $r^{\pi/2(m+1)\phi}$, the latter being required to be negligible for small r.

(B) Small angles: $\phi < \pi m/4(m+1)$.

In this case, if $u > 0$ holds initially local to the corner then the separable form

$$u \sim t^{-1/m} r^{2/m} G(\theta) \quad \text{as} \quad r \to 0 \tag{63}$$

will typically describe the local behaviour (though waiting-time behaviour is also possible there, depending on the local behaviour of the initial data; see subsection 5.6 for some relevant considerations); $G(\theta)$ is determined uniquely via $G(\pm\phi) = 0$ and its existence is readily demonstrated by phase-plane arguments.

It is worth recording the limiting properties of G in (63), which satisfies, on exploiting symmetry,

$$\frac{d}{d\theta}\left(G^m \frac{dG}{d\theta}\right) + \frac{4(m+1)}{m^2} G^{m+1} = -\frac{1}{m} G \quad \text{on} \quad 0 < \theta < \phi$$

$$\frac{dG}{d\theta} = 0 \quad \text{on} \quad \theta = 0, \qquad G = 0 \quad \text{on} \quad \theta = \phi.$$

We now disregard the second boundary condition, viewing this as a shooting problem with shooting parameter $G(0)$, and address the two limiting cases. Firstly, setting $G(0) = \varepsilon$ with $0 < \varepsilon \ll 1$, the rescaling $\theta = \varepsilon^{m/2}\Theta$ leads at leading order to

$$\frac{d}{d\Theta}\left(G_0^m \frac{dG_0}{d\Theta}\right) = -\frac{1}{m} G_0$$

equivalent to (29), providing the $\phi \to 0$ behaviour (with $\varepsilon = O(\phi^{2/m})$) and making a natural connection with the behaviour in slender domains. The converse case, $G(0) = 1/\varepsilon$, is best analysed in the w-formulation (8), with an application of the method of strained coordinates (see [17], for example) leading to

$$G \sim \frac{1}{\varepsilon}\left[\cos\left(\frac{2(m+1)}{m}(1+\sigma\varepsilon^m)\theta\right)\right]^{1/(m+1)} \tag{64}$$

where the constant σ satisfies

$$\sigma \sim \frac{m}{4(m+1)^2\pi}\mathcal{B}\left(\frac{1}{2}, \frac{2m+3}{2(m+1)}\right) \qquad \text{as} \quad \varepsilon \to 0$$

follows from the resulting solvability condition, with $\mathcal{B}(\cdot,\cdot)$ being the Beta function. Hence

$$\phi \sim \phi_c\left(1 - \sigma\varepsilon^{m+1}\right),$$

i.e. this limit is associated with $\phi \to \phi_c^-$, and (64) describes an intuitive transition to (62).

5.4. **Corner filling.** As we have already noted, for $\phi < \phi_c$, if $u \equiv 0$ holds at $t = 0$ about the corner then the associated hole is not fully closed in finite time. Rather, the conservation law associated with

$$\Phi = r^{-\pi/2\phi}\cos\left(\frac{\pi\theta}{2\phi}\right) \tag{65}$$

comes into play, the difference in sign from (49) being crucial ((65) applies in case (A) above too prior to hole closure, but the information it provides in this case is of limited value). This conservation law implies the existence of a local ('inner') first-kind similarity solution

$$u \sim t^{-\alpha}g\left(\rho,\theta\right), \qquad \rho = rt^{\beta} \tag{66a}$$

with

$$\alpha = \frac{\pi - 4\phi}{m\pi - 4(m+1)\phi} \qquad \beta = \frac{2\phi}{m\pi - 4(m+1)\phi} \tag{66b}$$

for $t \to \infty$ with $\rho = O(1)$. This solution must have far-field behaviour (63) as $\rho \to \infty$ that corresponds to the near-field behaviour of the 'outer' solution (50), again reflecting appropriate matching in the usual sense of matched-asymptotic expansions. Expressions (63) and (65) lead to a further derivation of ϕ_c (in addition to that implicit in the similarity variables in (66b)), the condition $\phi < \phi_c$ then being required for Φu to have finite integral over the domain when Φ is given by (65) and u by (66a), the inner region giving the dominant contribution to the associated conserved quantity.

In (48), κ can be identified with ϕ/ε for small ϕ so these expressions correspond to

$$r \propto t^{-2\phi/(m\pi)},$$

consistent with the small ϕ limit of (66a). By contrast, for $\phi > \phi_c$ the moving boundary necessarily reaches $r = 0$ in finite time when $u \equiv 0$ holds locally at $t = 0$; how it does so raises interesting open questions that we do not seek to address here, though a natural conjecture is that the moving boundary has $r = O((t_c - t)^{\beta})$ for some (second-kind) $\beta > 0$ as t approaches the hole-closure time t_c.

Here we provide a numerical demonstration of both cases, $\phi < \phi_c$ and $\phi > \phi_c$, in Figure 12, illustrating the evolution with the corner distanced from the support of u_0; with the figure we also show the resulting time dependencies of the mid-points of both interfaces, in keeping with the self-similar forms identified in (50b) and (66a).

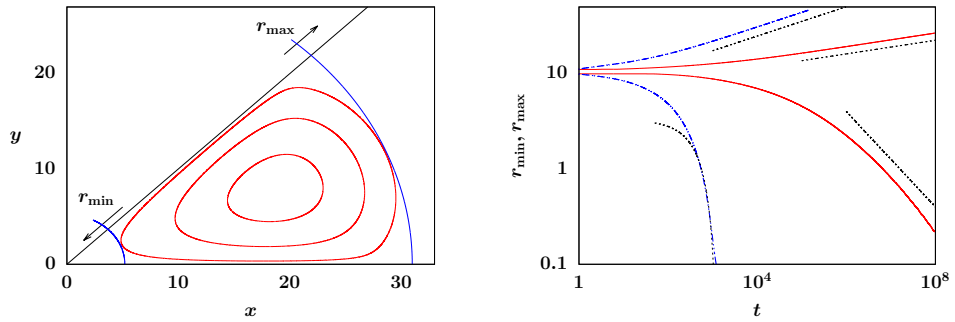

FIGURE 12. (left) Schematic showing definitions of $r_{\min}(t)$ and $r_{\max}(t)$ for the region of support of the spreading solution in a sector with $\phi = \pi/8$, corresponding to the left-hand panel of Figure 10. (right) Simulation results for $r_{\min}, r_{\max}$ for $m = 3/4$ (blue dashed curves) and $m = 2$ (red solid curves) along with the asymptotic predictions (black dotted curves): infinite time spreading for $m > m_c$ and finite-time corner-filling for $m < m_c$, where $m_c = 1$ for $\phi = \pi/8$. The three infinite-time predictions are those obtained from the first-kind solutions; the finite-time one (for $r_{\min}$ with $m < m_c$) is a fit to an a priori unknown power law, $r \propto (t_c - t)^{\gamma}$.

5.5. **Linear and fast diffusion.** In the linear case $m = 0$[2], one way to construct the large-time behaviour is by first setting

$$u = r^{\pi/2\phi} \cos\left(\frac{\pi\theta}{2\phi}\right) \Psi,$$

to give

$$\frac{\partial \Psi}{\partial t} = \frac{\partial^2 \Psi}{\partial r^2} + \frac{\pi + \phi}{\phi r} \frac{\partial \Psi}{\partial r},$$

equivalent to the radially symmetric heat equation in dimension $(\pi + 2\phi)/\phi$, so in this sense drainage through the fixed boundary is equivalent to the geometric spreading that becomes more pronounced with increasing dimension (corresponding to decreasing ϕ). Hence

$$\Psi \sim K t^{-(\pi+2\phi)/2\phi} e^{-r^2/4t} \quad \text{as} \quad t \to +\infty \quad \text{with} \quad r = O(t^{1/2}),$$

with u then corresponding to (50) with $m = 0$.

The result (50) implies that a first-kind solution for fast diffusion ($m < 0$) persists for $m > -4\phi/(\pi + 4\phi)$ and we expect (by analogy with the Cauchy problem in dimension greater than two – see [20]) that for $-1 < m < -4\phi/(\pi + 4\phi)$ the conservation law fails due to a non-zero flux to infinity and finite-time extinction occurs described by second-kind self-similarity. We again leave such questions open here, though see [21] for some discussion of the $\phi = \pi/2$ case. It is noteworthy that no transition of this type occurs in the Cauchy problem in two dimensions. The transition that occurs for slow diffusion ($m > 0$) at $\phi = \phi_c$ similarly has no analogue in the Cauchy problem, emphasising the special status of wedges in capturing such a transition.

[2]See also [23].

5.6. **Waiting-time behaviour.** We conclude our discussion of $m > 0$ by giving one further derivation of ϕ_c, noting its relevance to waiting-time phenomena. We consider initial conditions of the form

$$u_0 \sim r^{2/m}\psi_0(\theta) \quad \text{as} \quad r \to 0$$

for some prescribed $\psi_0(\theta)$ and set

$$u \sim r^{2/m}\psi(\theta, t) \quad \text{as} \quad r \to 0$$

for sufficiently small t to give

$$\begin{gathered} \frac{\partial \psi}{\partial t} = \frac{\partial}{\partial \theta}\left(\psi^m \frac{\partial \psi}{\partial \theta}\right) + \frac{4(m+1)}{m^2}\psi^{m+1}, \\ \psi = 0 \qquad \text{on} \quad |\theta| = \phi, \\ \psi = \psi_0(\theta) \qquad \text{at} \quad t = 0, \end{gathered} \tag{67}$$

which is meaningful in its own right as a one-dimensional reaction-diffusion problem, a viewpoint that we pursue before reinterpreting the results in terms of the two-dimensional problem. The intermediate asymptotic behaviour of (67) can be summarised as follows:

$$\phi < \phi_c \quad \psi \sim t^{-1/m}G(\theta) \quad \text{as} \quad t \to +\infty, \tag{68}$$

$$\phi = \phi_c \quad \psi^{m+1} \sim K\cos\left(\frac{2(m+1)}{m}\theta\right) \quad \text{as} \quad t \to +\infty, \tag{69}$$

$$\phi_c < \phi < \frac{\pi}{2} \quad \psi \sim (t_c - t)^{-1/m}G(\theta) \quad \text{as} \quad t \to t_c^- \tag{70}$$

$$\phi > \frac{\pi}{2} \quad \psi \sim \frac{m}{2(m+2)}(t_c - t)^{-1/m}\cos^2(\theta - \theta_c) \quad \text{as } t \to t_c^-, \text{ with } \quad |\theta - \theta_c| < \frac{\pi}{2}, \tag{71}$$

where the constants K, t_c and θ_c depend on the initial data; K can be expressed in terms of $\psi_0(\theta)$ using an obvious conserved quantity, and the constraint $|\theta_c| < \phi - \pi/2$ applies. Hence finite-time blow-up of ψ occurs for large-enough domains, $\phi > \phi_c$; the boundary value problems governing $G(\theta)$ in each of (68) and (70) can be inferred directly from (67). For $\phi > \pi/2$ finite-time blow-up is restricted to the range $|\theta - \theta_c| < \pi/2$, further insight into which can be gleaned by co-opting a solution from [19], whereby

$$\psi^m = (A(t)\cos^2\theta - B(t)\sin^2\theta)_+ \tag{72}$$

with

$$\begin{aligned} A(t) &= \frac{A_0}{(1 - 4A_0T/m)^{(m+2)/2}(1 + 4B_0T/m)^{m/2}}, \\ B(t) &= \frac{B_0}{(1 - 4A_0T/m)^{m/2}(1 + 4B_0T/m)^{(m+2)/2}} \end{aligned}$$

where $A_0 = A(0)$, $B_0 = B(0)$ and T is defined by

$$t = \int_0^T \left(1 - \frac{4A_0T'}{m}\right)^{m/2}\left(1 + \frac{4B_0T'}{m}\right)^{m/2} dT';$$

the invariant subspace (72) may alternatively be written in the form $\psi^m = (a(t) + b(t)\cos 2\theta)_+$.

Returning now to the two-dimensional problem, (71) is simply a one-dimensional solution, while (72) corresponds to $u^m = (A(t)x^2 - B(t)y^2)_+$. We have already noted the role of (68), with the steady state (69) confirming the critical value ϕ_c. The

existence of a suitable $G(\theta)$ in (70), as well as in (68), follows from a phase-plane analysis. The finite-time blow-up in (70) and (71) is associated with a waiting-time phenomenon (cf. [24]), with the local behaviour switching to (62) at some finite time $t \leq t_c$. That (71) does not blow up over the entire range of θ implies a novel class of waiting-time behaviour; (72) further generalises this in that the support of u involves an increasing angular range until it either collides with the fixed boundaries (for $\phi < \pi/2$) or finite-time blow-up is manifest over $|\theta| < \pi/2$ (for $\phi > \pi/2$; the solution (72) can of course be generalised by translating θ by a constant, cf. (71)).

6. **Discussion.** Our focus in this concluding section is largely on open problems, starting with those we have explored above by formal methods and which warrant more rigorous investigation.

- Confirmation of the various types of intermediate-asymptotic behaviour elucidated above for the two classes of phenomena implicit in Figures 1 and 2, including identification of the critical angle demarcating finite- and infinite-time hole closure.
- Clarification of the roles of first- and second-kind self-similarity in the case of sign-change solutions.
- Confirmation of the proposed critical exponents and associated finite-time extinction behaviour for fast-diffusion.
- Confirmation of the transition in local behaviour at $\phi = \phi_c$ outlined in Sections 5.3-5.4 (compare [5], Chapter 10, for similar behaviour in linear problems).

Natural extensions not described above even in formal terms include the following.

- Higher-dimensional problems (the formal analysis has been extended to conical domains, but is not reported here; additional qualitative phenomena arise).
- The intermediate-asymptotic behaviour of finite-time hole closure on the boundary for zero-Dirichlet boundary conditions (contrast [2] for the Cauchy problem, from which zero-Neumann results can be inferred) at regular, as well as singular, points on the fixed boundary. Radially symmetric solutions are not, of course, available in this case.
- The limit $\phi \to \infty$, complementary to the slender-domain case. This can be (and has been, [22]) addressed by formal-asymptotic methods (requiring a solvability-condition argument to determine an angular-dependent prefactor to the radial dependence of near-source-solution type). The results are not reported in view of their limited physical relevance, but it is worth highlighting that the slit limit $\phi \to \pi^-$ is not a singular one (in contrast to what might be expected from other 'slender-body' contexts), with $\phi = \pi$ playing no distinguished role.

Finally, more open-ended issues include the following two.

- Very natural generalisations include those to the p-Laplacian and doubly nonlinear second-order parabolic equations,

$$\frac{\partial u}{\partial t} = \nabla \cdot (|\nabla u|^{p-2}\nabla u), \quad \frac{\partial u}{\partial t} = \nabla \cdot (u^m |\nabla u|^{p-2}\nabla u),$$

and to the thin-film equation,

$$\frac{\partial h}{\partial t} = -\nabla \cdot (h^n \nabla \Delta h). \tag{73}$$

However, for none of these can the time-derivative be written as the Laplacian of some quantity, and the only associated conservation law is in general the mass, requiring the application of second-kind self-similarity in the analogues of almost all the problems above. One exception is (73) with $n = 1$, for which first moments are conserved, [8], enabling progress with the dipole problem at least; however, as is well-known, many additional difficulties accrue with higher-order cases such as (73).

- Corrections to the intermediate-asymptotic behaviour associated with perturbations to wedges in the far- or near-field could be pursued (i.e. fixed boundaries $|\theta| = \phi + o(1)$ as $r \to \infty$ or $r \to 0$; this has been partially investigated though results are again omitted).

Appendix A. **Diffusion in three-dimensional cylinders.** Here we step outside the framework set in the introduction to consider the porous medium equation in three dimensions subject to Robin boundary conditions. We consider infinite cylinders whose cross-section occupies for each x a region Ω parallel to the (y, z) plane where Ω is independent of x. We shall address this case only briefly, focussing on a specific limit, spelling out in Section 3 the two-dimensional case in more detail, this being the setting we pursue in the remainder of the paper. We write

$$\frac{\partial u}{\partial t} = \nabla \cdot (u^m \nabla u) + \frac{\partial}{\partial x}\left(u^m \frac{\partial u}{\partial x}\right) \tag{74}$$

with $\nabla = (\partial/\partial y, \partial/\partial z)$ and take $u \to 0$ as $|x| \to \infty$, with

$$\frac{\partial u}{\partial \nu} = -\mu u, \quad \mu > 0 \tag{75}$$

holding on $\partial\Omega$, $\partial/\partial\nu$ being the outward normal derivative, this generalisation of the case $\mu = \infty$[3] proving instructive: in particular, the limit $\mu \to 0$ leads to a much more tractable problem that allows rather general lessons to be drawn.

Setting $t = \hat{t}/\mu$ and $x = \hat{x}/\sqrt{\mu}$, we can expand the solution $u = u(\hat{x}, y, z, \hat{t}\,)$ for $\mu \to 0$ as $u = u_0 + \mu u_1 + O(\mu^2)$. Using a standard long-wave asymptotic approach, it can be shown that u_0 is independent of the transverse variables, $u_0 = u_0(\hat{x}, \hat{t}\,)$. At next order we obtain a solvability condition on u_0 that can be re-written in the original variables as

$$\frac{\partial u}{\partial t} \sim \frac{\partial}{\partial x}\left(u^m \frac{\partial u}{\partial x}\right) - \frac{\mu L}{A} u^{m+1},$$

where A is the area of Ω and L the arclength of $\partial\Omega$. We therefore now analyse this one-dimensional problem in its simplest rescaled form: this will prove instructive for the analysis of the more general case. Hence we consider the reaction-diffusion equation

$$\frac{\partial u}{\partial t} = \frac{\partial}{\partial x}\left(u^m \frac{\partial u}{\partial x}\right) - u^{m+1} \tag{76}$$

with $u \to 0$ as $|x| \to \infty$ and exploit a known class of explicit solutions (see (79) and (85) below) alongside the divergence form

$$\frac{\partial}{\partial t}(\Phi u) = \frac{\partial}{\partial x}\left(\Phi u^m \frac{\partial u}{\partial x} - \frac{1}{m+1} u^{m+1} \frac{\partial \Phi}{\partial x}\right) \tag{77}$$

[3]This case, and other generalisations thereof, has also been analysed in [11], work of which we became aware subsequent to the completion of the current analysis.

and the resulting conservation laws that arise for

$$\Phi = e^{\pm(m+1)^{1/2}x}, \tag{78}$$

in effect drawing on and generalising results from [25,26]. While the explicit solutions correspond to specific initial conditions, their large-time limits describe generic intermediate-asymptotic behaviour, making them of general relevance.

Setting $v = u^m$ in (76) leads to the quadratically nonlinear form (cf. (5))

$$\frac{\partial v}{\partial t} = v\frac{\partial^2 v}{\partial x^2} + \frac{1}{m}\left(\frac{\partial v}{\partial x}\right)^2 - mv^2$$

and it is now appropriate to subdivide the analysis between the cases $m > 0$ and $-1 < m < 0$. Thus, for $m > 0$ we set

$$v = (A(t) - B(t)\cosh(mx/(m+1)^{1/2}))_+, \quad 0 < B < A, \tag{79}$$

to obtain

$$\frac{dA}{dt} = -mA^2 - \frac{m}{m+1}B^2, \quad \frac{dB}{dt} = -\frac{m(m+2)}{m+1}AB \tag{80}$$

implying

$$A = B\left(1 + K^2 B^{-2/(m+2)}\right)^{1/2} \tag{81}$$

for constant K, and $B(t)$ can then be expressed implicitly in terms of a hypergeometric function. More importantly here, for $m > 0$ we have $B \to 0$ with $B \ll A$ as $t \to +\infty$ so that

$$A \sim \frac{1}{mt}, \quad B \sim \frac{1}{(Kmt)^{(m+2)/(m+1)}} \quad \text{as} \quad t \to +\infty \tag{82}$$

and the edges of the support of u thus satisfy

$$|x| \sim \frac{1}{m(m+1)^{1/2}}\ln t \quad as \quad t \to +\infty, \tag{83}$$

a result that also follows directly from the consequence

$$\frac{d}{dt}\left(\int_{-\infty}^{\infty} \Phi u\, dx\right) = 0 \tag{84}$$

of (77), given (78).

The behaviour for $-1 < m < 0$, for which the sink term in (76) is non-Lipschitz, differs significantly (the solution extinguishes instantly for $m \le -1$). Now from

$$v = A(t) + B(t)\cosh\left((-m)x/(1+m)^{1/2}\right), \quad A, B > 0 \tag{85}$$

we recover (80)-(81); however, $A, B \to \infty$ now applies as $t \to t_c^-$ for some finite extinction time t_c, so that $A \sim B$ and hence

$$A, B \sim \frac{1+m}{(-m)(2+m)}\frac{1}{t_c - t} \quad \text{as} \quad t \to t_c^-.$$

Hence the solution approaches a separable form as $t \to t_c^-$, with the conservation law (84) no longer applying due to the 'flux'

$$-\Phi u^m \frac{\partial u}{\partial x} + \frac{1}{1+m}u^{1+m}\frac{\partial \Phi}{\partial x}$$

to $+\infty$ being positive (and finite) for the appropriate choice of sign in (78) (and similarly at $-\infty$ with the obvious changes of sign).

The availability of the above classes (79) and (85) of exact solution make the analysis of (76) particularly transparent and provide insights that carry over to the less tractable fully two-dimensional problem (see Section 3), as does the role of conservation laws of a less familiar type than those exploited in Section 2.2. In summary, the following classes of intermediate-asymptotic behaviour arise in the above.

(*i*) $m > 0$

$$u^m \sim \frac{1}{mt} \quad \text{as} \quad t \to +\infty \quad \text{with} \quad x = O(1) \tag{86}$$

$$u^m \sim \frac{1}{mt}\left(1 + \frac{1}{2K^{(m+2)/(m+1)}m^{1/(m+1)}} \exp\left(\frac{mz}{(m+1)^{1/2}}\right)\right) \quad \text{as} \quad t \to +\infty \quad \text{with} \quad z = O(1) \tag{87}$$

where $z = x - q\ln t$ with $q = 1/(m\sqrt{m+1}\,)$, and K can be expressed in terms of the initial data using (84); an equivalent expression holds for $x + q\ln t = O(1)$. For the invariant subspace (79) of solutions we have

$$\begin{aligned}\int_{-\infty}^{\infty} \Phi u\, dx &= \frac{2^{(m+1)/m}(m+1)^{1/2}}{m}\mathcal{B}\left(\frac{m+1}{m}, \frac{m+1}{m}\right)\frac{(A^2 - B^2)^{(m+2)/2m}}{B^{(m+1)/m}} \\ &= \frac{2^{(m+1)/m}(m+1)^{1/2}}{m}\mathcal{B}\left(\frac{m+1}{m}, \frac{m+1}{m}\right)K^{(m+2)/m},\end{aligned}$$

where $\mathcal{B}(\cdot,\cdot)$ again denotes the Beta function. We note that

$$u = t^{-1/m} f(x - q\ln t)$$

constitutes a classical similarity reduction of (76), associated with the latter's invariance under simultaneous rescalings of u and t and translations of x, and is of a type that appears in Section 3.

(*ii*) $m = 0$

$$u \sim Kt^{-1/2}e^{-t}e^{-x^2/4t} \quad \text{as} \quad t \to +\infty \quad \text{with} \quad x = O(t^{1/2}), \tag{88}$$

holds in the linear case, which is borderline in nature; K can be determined from the mass of the initial data.

(*iii*) $-1 < m < 0$

$$u^m \sim \frac{1}{t_c - t}\frac{1+m}{(-m)(2+m)}\left(1 + \cosh((-m)x/(1+m)^{1/2})\right) \quad \text{as} \quad t \to t_c^- \quad \text{with} \quad x = O(1), \tag{89}$$

i.e. separable behaviour of non-trivial spatial structure (contrast (86)) provides the full story. The most significant more general lesson to be drawn from this case is the failure of the putative conserved quantities due to the finite flux to infinity.

Returning now to the case of arbitrary μ in (74)-(75) the relevant conservation laws are given by

$$\Phi = e^{\pm\lambda z}\phi(x,y) \tag{90}$$

with ϕ and the possible values of λ being determined by the eigenvalue problem

$$\begin{aligned}\nabla^2\phi &= -\lambda^2\phi \quad \text{in } \Omega \\ \frac{\partial\phi}{\partial\nu} &= -(m+1)\mu\phi \quad \text{on } \partial\Omega\end{aligned} \tag{91}$$

so that

$$\frac{\partial}{\partial t}(\Phi u) = \nabla \cdot \left(\Phi u^m \nabla u - \frac{1}{m+1} u^{m+1} \nabla \Phi \right) + \frac{\partial}{\partial z} \left(\Phi u^m \frac{\partial u}{\partial z} - \frac{1}{m+1} u^{m+1} \frac{\partial \Phi}{\partial z} \right) \tag{92}$$

and

$$\frac{d}{dt} \int_{-\infty}^{\infty} \Phi u \, dx \, dy \, dz = 0 \tag{93}$$

provided the flux to infinity associated with (92) is zero. We shall be concerned here only with the smallest positive eigenvalue in (90) since this governs the large-time behaviour for $m > 0$.

For $\mu = 0$ we have $\lambda = 0$, $\phi = 1$, and the $t \to +\infty$ behaviour for $m > -2$ is then one dimensional in z and given by the one-dimensional Barenblatt-Pattle (i.e. source) self-similar solution (for $-2 < m \leq -1$, non-maximal solutions are also possible, as discussed by [28]; for $\mu > 0$ this is no longer the case, $m > -1$ being required for existence).

We do not have an explicit solution to deploy in this more general case, but can still appeal to a conservation-law argument based on (93) and akin to that exploited above. Thus as $t \to +\infty$ the following asymptotic structure arises for $m > 0$

$$u \sim t^{-1/m} f(x, y) \quad \text{for} \quad z = O(1), \tag{94}$$

$$u \sim t^{-1/m} g(x, y, z - q \ln t) \quad \text{for} \quad z = q \ln t + O(1), \tag{95}$$

with equivalent behaviour to (95) for $z = -q \ln t + O(1)$; in (95) the wavespeed q is a constant given by (96) below, and f and g constitute exact self-similar reductions of (74), each satisfying an elliptic boundary-value problem (a free boundary problem in the case of g) that can be derived in the usual way (with $f(x, y) = g(x, y, -\infty)$). For the upper sign in (90) (with $\lambda > 0$) the integral in (93) is dominated by (95), implying that

$$q = \frac{1}{m\lambda} \tag{96}$$

where λ is the smallest positive eigenvalue from the linear eigenvalue problem (91).

By contrast, for $-1 < m < 0$ the intermediate asymptotic solution is (by immediate analogy with the one-dimensional reduced model above) separable everywhere:

$$u \sim (t_c - t)^{1/(-m)} f(x, y, z) \quad \text{as} \quad t \to t_c^-$$

for some positive constant t_c. Indeed, the left-hand-side of (74) is negligible as $|z| \to \infty$ so that

$$u^{1+m} \sim a(t) e^{-\lambda z} \phi(x, y) \quad \text{as} \quad z \to +\infty \tag{97}$$

(and similarly as $z \to -\infty$) for some function $a(t)$, λ again being the smallest positive eigenvalue: the flux to infinity associated with (92) is positive and the integral in (93) tends to zero as $t \to t_c^-$. That the case $\mu = \lambda = 0$ is a singular limit is evident from (97), and from the fact that $q \to \infty$ in (96) as $\mu \to 0$, so that $\lambda \to 0$.

Appendix B. **Properties of the half-plane similarity solution.** Here we show how local asymptotic expansions can be employed in order to gain insight into the structure of self-similar solutions on the half-plane. We express the solution of (51) in rectangular coordinates, with $V(\xi, \eta)$, for the half-plane case (54),

$$-\frac{3m}{3m+2} V - \frac{1}{3m+2} \left(\eta \frac{\partial V}{\partial \eta} + \xi \frac{\partial V}{\partial \xi} \right) = V \left(\frac{\partial^2 V}{\partial \eta^2} + \frac{\partial^2 V}{\partial \xi^2} \right) + \frac{1}{m} \left(\left[\frac{\partial V}{\partial \eta} \right]^2 + \left[\frac{\partial V}{\partial \xi} \right]^2 \right). \tag{98}$$

As described by [14], the similarity profile is an even function of η, so in the region of support, $V(\xi,\eta) \sim \sum_{k=0}^{\infty} V_k(\xi)\eta^{2k}$ for $\eta \to 0$. The leading order term $V_0(\xi)$ is the centreline profile and passes through the maximum of V; it satisfies the equation

$$-\frac{3m}{3m+2}V_0 - \frac{1}{3m+2}\xi V_0' = V_0(V_0'' + 2V_1) + \frac{1}{m}\left(V_0'\right)^2. \tag{99}$$

We will present numerical results for the centreline profile (see Figure 13), but first we consider local behaviours near the fixed boundary and the edge of support.

To obtain a finite flux out through the boundary $\xi = 0$, $J(\eta) = U^m U_\xi = (V^{1/m}V_\xi)/m$, we require that

$$V \sim A(\eta)\xi^{m/(m+1)} \quad \text{as} \quad \xi \to 0^+, \tag{100}$$

where $A(\eta) = [(m+1)J(\eta)]^{m/(m+1)}$, as in (4). Given the symmetry about the centreline $\eta = 0$, we can expand $A(\eta) \sim \sum_{j=0}^{\infty} A_j \eta^{2j}$. We note that the expression (100) is valid only for $m > -1$, and that $J(\eta)$ is a positive quantity, describing draining flows. Extending to higher order terms gives in both ξ and η

$$V \sim A_0\xi^{m/(m+1)} - \frac{m(m+1)(3m+4)}{(m+2)(2m+3)(3m+2)}\xi^2 + A_1\eta^2\xi^{m/(m+1)} - \frac{A_1}{3}\xi^{(3m+2)/(m+1)}. \tag{101}$$

Alternatively, we can set $V(\xi,\eta) = \mathcal{A}(\xi,\eta)\xi^{m/(m+1)}$; while the full PDE for $\mathcal{A}$ is more cumbersome than (98), if we seek to calculate just the leading order and first correction (at $O(\xi^2)$) terms as $\xi \to 0$, it is sufficient to consider the reduced (and parabolic) equation

$$-\frac{m(3m+4)}{(m+1)(3m+2)}\xi^{m/(m+1)}\mathcal{A} - \frac{\eta\xi^{m/(m+1)}}{3m+2}\mathcal{A}_\eta = \xi^{2m/(m+1)}\mathcal{A}\mathcal{A}_{\xi\xi} + 2\eta^{(m-1)/(m+1)}\mathcal{A}\mathcal{A}_\xi,$$

which can be rewritten as

$$\xi^2\mathcal{A}_{\xi\xi} + 2\xi\mathcal{A}_\xi = -\frac{m(3m+4)}{(m+1)(3m+2)}\xi^{(m+2)/(m+1)} - \frac{\eta}{3m+2}\eta^{(m+2)/(m+1)}\frac{\mathcal{A}_\eta}{\mathcal{A}}.$$

This is essentially an inhomogeneous Cauchy-Euler differential equation with respect to derivatives in ξ and has general solution of the form

$$\mathcal{A} = A(\eta) + \frac{B(\eta)}{\xi} + O(\xi^{(m+2)/(m+1)}) \qquad \xi \to 0.$$

In order to have finite flux through $\xi = 0$, $B(\eta)$ must vanish, but there are no local restrictions on the form of $A(\eta)$. Then assuming that $\mathcal{A}$ is smooth with $\mathcal{A}, \mathcal{A}_\eta = O(1)$ as $\xi \to 0$ this solution can be expressed as

$$\mathcal{A}(\xi,\eta) = A(\eta) - \frac{m(m+1)(3m+4)}{(m+2)(2m+3)(3m+2)}\xi^{(m+2)/(m+1)} + O(\eta^2\xi^{(m+2)/(m+1)}), \tag{102}$$

for $\xi, \eta \to 0$, which is consistent with (101). Importantly, this result makes explicit that the dependence on η cannot be determined just by local considerations and is coupled to the global structure of the solution.

Away from singular triple points where the moving boundary meets the fixed boundary, the local expansion of the solution at the interface can be obtained. In

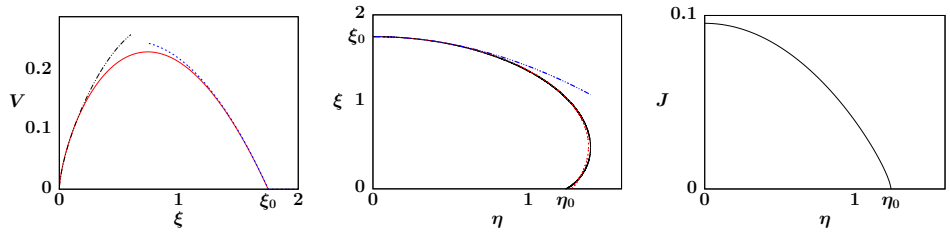

FIGURE 13. (left) Centreline profile $V(\xi,0)$ for the $m=2$ half-plane similarity solution (solid red) compared with the two-term local expansions at $\xi=0$ (101) (dash-dotted black) and at the tip $\xi=\xi_0$ (103) (dashed blue), (middle) Half-view of the free-boundary (solid black) compared with local quadratic form at the tip (104) (dash-dotted blue) and also fitted to a shifted ellipse (105) (dashed red), and (right) The flux $J(\eta)$ (see (100)) through the fixed boundary $\xi=0$.

particular at the leading "tip" of the support ($\xi=\xi_0$), on the centreline we have

$$V \sim \frac{m\xi_0}{3m+2}(\xi_0-\xi) - \frac{m}{2(1+m)}\left(\frac{3m+1}{3m+2}-2C_0\right)(\xi_0-\xi)^2 - C_0\eta^2, \qquad (103)$$

for $\xi\to\xi_0^-$ and $\eta\to 0$ with some constant $C_0>0$ (giving the finite η-curvature of the solution as $\xi\to\xi_0^-$); this result is consistent with (53). The expression (103) also implies that the shape of the interface local to the tip takes the form

$$\xi \sim \xi_0 - \frac{(3m+2)C_0}{m\xi_0}\eta^2 \quad \text{as} \quad \eta\to 0. \qquad (104)$$

Figure 13 shows comparisons of these local expansions against the numerically computed similarity solution. We also observe that the free boundary of the solution roughly resembles a shifted ellipse,

$$\left(\frac{\xi-\xi_s}{a}\right)^2 + \left(\frac{\eta}{b}\right)^2 = 1, \qquad (105)$$

the major axis of interface being in the ξ-direction (normal to the boundary), while the interface is widest at some $\xi_s>0$. While this is a heuristic observation only, a numerically fitted ellipse is found to be a good approximation around most of the interface, though it deviates near $\eta=\eta_0$. Figure 13 also shows the profile for the flux out through $\xi=0$, $J(\eta)=U^mU_\xi|_{\xi=0}$.

Acknowledgments. We thank the reviewer for their valuable comments that helped us to improve the manuscript. MB thanks Joost Hulshof for helpful discussions on [14], and acknowledges support of the Waseda University Tokutei Kadai grants 2018B-104 and 2022R-031. TPW acknowledges support from grant NSF DMS 2008255. JRK gratefully acknowledges funding from the Leverhulme Trust in the form of a Fellowship.

REFERENCES

[1] S. B. Angenent and D. G Aronson, Optimal asymptotics for solutions to the initial value problem for the porous medium equation, *Nonlinear Problems in Applied Mathematics*, (1996), 10-19.

[2] S. B. Angenent, D. G. Aronson, S. I. Betelu and J. S. Lowengrub, Focusing of an elongated hole in porous medium flow, *Phys. D*, **151** (2001), 228-252.
[3] D. G. Aronson and L. A. Peletier, Large time behaviour of solutions of the porous medium equation in bounded domains, *J. Differential Equations*, **39** (1981), 378-412.
[4] G. I. Barenblatt, On some unsteady motions of a fluid and a gas in a porous medium, *Prikl. Mat. Makh.*, **16** (1952), 67-78.
[5] G. I. Barenblatt, *Similarity, Self-Similarity, and Intermediate Asymptotics*, Consultants Bureau [Plenum], New York-London, 1979.
[6] G. I. Barenblatt, *Scaling, Self-Similarity, and Intermediate Asymptotics: Dimensional Analysis and Intermediate Asymptotics*, Cambridge University Press, 1996.
[7] J. Bear, *Dynamics of Fluids in Porous Media*, Dover, 1988.
[8] S. I. Betelú and J. R. King, Explicit solutions of a two-dimensional fourth-order nonlinear diffusion equation, *Math. Comput. Modelling*, **37** (2003), 395-403.
[9] A. Friedman and S. Kamin, The asymptotic behavior of gas in an n-dimensional porous medium, *Trans. Amer. Math. Soc.*, **262** (1980), 551-563.
[10] J. Gilchrist, Flux diffusion and the porous medium equation, *Phys. C*, **291** (1997), 132-142.
[11] B. H. Gilding and J. Goncerzewicz, The porous media equation in an infinite cylinder, between two infinite parallel plates, and like spatial domains, *Interfaces and Free Boundaries*, **18** (2016), 45-73.
[12] J. Hulshof, Similarity solutions of the porous medium equation with sign changes, *J. Math. Anal. Appl.*, **157** (1991), 75-111.
[13] J. Hulshof, J. R. King and M. Bowen, Intermediate asymptotics of the porous medium equation with sign changes, *Adv. Differential Equations*, **6** (2001), 1115-1152.
[14] J. Hulshof and J. L. Vázquez, The dipole solution for the porous medium equation in several space dimensions, *Ann. Scuola Norm. Sup. Pisa Cl. Sci. (4)*, **20** (1993), 193-217, http://www.numdam.org/item/?id=ASNSP_1993_4_20_2_193_0.
[15] S. Kamin and J. L. Vazquez, Asymptotic behaviour of solutions of the porous medium equation with changing sign, *SIAM J. Math. Anal.*, **22** (1991), 34-45.
[16] W. L. Kath and D. S. Cohen, Waiting-time behavior in a nonlinear diffusion equation, *Stud. Appl. Math.*, **67** (1982), 79-105.
[17] J. Kevorkian and J. D. Cole. *Perturbation Methods in Applied Mathematics*, volume 34 of *Applied Mathematical Sciences*. Springer-Verlag, New York-Berlin, 1981.
[18] J. R. King, Integral results for nonlinear diffusion equations, *J. Engrg. Math.*, **25** (1991), 191-205.
[19] J. R. King, Exact multidimensional solutions to some nonlinear diffusion equations, *Quart. J. Mech. Appl. Math.*, **46** (1993), 419-436.
[20] J. R. King, Self-similar behaviour for the equation of fast nonlinear diffusion, *Philos. Trans. R. Soc. Lond. Ser. A Math. Phys. Eng. Sci.*, **343** (1993), 337-375.
[21] J. R. King, Asymptotic analysis of extinction behaviour in fast nonlinear diffusion, *J. Engrg. Math.*, **66** (2010), 65-86.
[22] J. R. King, Unpublished notes, 2021.
[23] R. C. Kloosterziel, On the large-time asymptotics of the diffusion equation on infinite domains, *J. Engrg. Math.*, **24** (1990), 213-236,
[24] A. A. Lacey, J. R. Ockendon and A. B. Tayler, "Waiting-time" solutions of a nonlinear diffusion equation, *SIAM J. Appl. Math.*, **42** (1982), 1252-1264.
[25] W. I. Newman, Some exact solutions to a nonlinear diffusion problem in population genetics and combustion, *J. Theoret. Biol.*, **85** (1980), 325-334.
[26] W. I. Newman, The long-time behavior of the solution to a nonlinear diffusion problem in population genetics and combustion, *J. Theoret. Biol.*, **104** (1983), 473-484.
[27] R. E. Pattle, Diffusion from an instantaneous point source with a concentration-dependent coefficient, *Quart. J. Mech. Appl. Math.*, **12** (1959), 407-409.
[28] A. Rodríguez and J. L. Vázquez, Non-uniqueness of solutions of nonlinear heat equations of fast diffusion type, *Ann. Inst. H. Poincaré Anal. Non Linéaire*, **12** (1995), 173-200.
[29] J. L. Vázquez, *Smoothing and Decay Estimates for Nonlinear Diffusion Equations*, volume 33 of *Oxford Lecture Series in Mathematics and its Applications*, Oxford University Press, Oxford, 2006.
[30] J. L. Vázquez, *The Porous Medium Equation*, Oxford University Press, Oxford, 2007.
[31] J. L. Vazquez, Porous medium flow in a tube: Traveling waves and KPP behavior, *Commun. Contemp. Math.*, **9** (2007), 731-751.

[32] T. P. Witelski and A. J. Bernoff, Self-similar asymptotics for linear and nonlinear diffusion equations, *Studies in Applied Mathematics*, **100** (1998), 153-193.
[33] T. P. Witelski and M. Bowen, ADI schemes for higher-order nonlinear diffusion equations, *Appl. Numer. Math.*, **45** (2003), 331-351.
[34] Y. B. Zel'dovič and G. I. Barenblatt, Asymptotic properties of self-preserving solutions of equations of unsteady motion of gas through porous media, In *Doklady Akademii Nauk*, volume 118, 671-674. Russian Academy of Sciences, 1958.
[35] Ya. B. Zeldovich and G. I. Barenblatt, On the dipole-type solution in the problems of a polytropic gas flow in porous medium, *Prikl. Mat. Mekh*, **21** (1957), 718-720.
[36] Ya. B. Zel'dovič and A. S. Kompaneets, On the theory of propagation of heat with the heat conductivity depending upon the temperature, In *Collection in Honor of the Seventieth Birthday of Academician A. F. Ioffe*, 61-71. Izdat. Akad. Nauk SSSR, Moscow, 1950.

Received March 2022; revised November 2022; early access December 2022.